Modification of the Microstructural Features and Hardness of γ-TiAl by Heat Treatments

Bachelor Thesis

Aerospace Engineering

Carlos III University of Madrid

Name:	Elena Martínez Lizuain
Tutor of the Thesis:	Ph. D. Elisa Mª Ruiz-Navas
Director of the Thesis	Ph. D. José Manuel Torralba Castelló
Subject:	Materials Science and Engineering
Due date:	24/09/2014

Universidad
Carlos III de Madrid

This bachelor thesis has been developed in the facilities of IMDEA Materials Institute and Carlos III University of Madrid.

Acknowledgments

I wish to express my gratitude to my tutor of the thesis, Ph. D. Elisa Mª Ruiz Navas, for help with the completion of this project and her encouragement to submerge myself in exploring the field of intermetallics, particularly of the gamma titanium aluminides which were unknown to me and have discovered me a really exciting subject. Moreover, I would like to thank her support to overcome all the difficulties that have appeared during the development of the experimental procedure of this thesis that have resulted in an incredible enrichment of our initial objectives. In short, thanks for letting your office be my second analysis laboratory!

I would also like to thank my director of the thesis, Ph. D. José Manuel Torralba for giving me the opportunity to participate in a project of the material science and engineering department and, I am hugely thankful that he offered me the chance to develop some of the project in IMDEA Materials Institute which has been an incredible experience. Likewise, I wish to thank all the people that have helped me there.

I would like to appreciate the continued support of Ph. D. Rocío Muñoz Moreno who since the first day has helped me with this bachelor thesis and has given me excellent advices to investigate γ-TiAl, to develop the experiments in the laboratory and to unravel some of the secrets that entails this alloy. Thank you for listen and answer my numerous doubts even from Cambridge!

In addition to this, I wish to thank Cristina Moral who has helped me endless hours in front of the SEM to obtain all the images that I needed. Thanks also to Francisco Javier González whose knowledge and experience with AFM had allowed me to successfully see the microstructure from a different point of view and have opened new possibilities for further research. Likewise, I really appreciate Grupo de Tecnologías de Polvos of Carlos III University who have always been willing to help with the using of the laboratory and all its equipment and handicaps. Thanks also to Sophia Tsipas and to my aerospace partners of thesis who have been an incredible support.

A special thanks to my parents, my brother and my friends for their continued support and encouragement. Thank you with all my heart!

Thank you all.

Abstract

γ-TiAl intermetallic alloys are very attractive materials for aerospace applications because of their excellent specific properties at high temperatures. Particularly, γ-TiAl alloys will replace the heavier Ni-based superalloys currently used for low pressure turbine (LPT) blades manufacturing.

The main objective of this research work is to study the microstructural evolution during heat treatments in a Ti-45Al-2Nb-2Mn (at.%) + 0.8 (vol.%) TiB_2 alloy (Ti4522XD). The alloy was initially processed through hot isostatic pressing (HIP) of prealloyed powder and centrifugal casting (CC). In order to generate a wide variety of microstructures, heat treatments were carried out at defined temperatures accordingly to the γ-TiAl phase diagram. Microstructural characterization was achieved by scanning electron microscopy (SEM) and atomic force microscopy (AFM). For the obtained micrographs, the colony and grain size were measured together with the volume fraction of the different phases and a first approach to lamellar spacing was performed. Furthermore, microhardness Vicker tests were carried out with the aim of analysing the resulting mechanical properties.

For these results, conclusions concerning the microstructure evolution of this alloy during heat treatments are drawn. It is proved that the γ-TiAl microstructure is highly sensitive to the heat treatments temperature. Highest hardness values are associated to microstructures composed by a balanced proportion of lamellar colonies and equiaxed grains. This is a first approach to establish a relationship between the microstructure and different heat treatments that can be complemented with defined further research.

Index

Motivation and objective

Material science is one of the areas playing a major role in the aerospace field to develop more environmentally-friendly and economic engineering solutions. With the introduction of composites, new aircraft dimensions and performances have been possible. However, an important effort should be also done in the development of more efficient engines. Engine components suffer of very aggressive environments at high temperatures where γ-TiAl alloys present very high capabilities (up to 750 °C). γ-TiAl alloys have already been implemented in the LPT blades of the new Dreamliner Boeing aircrafts. However, due to the complexity of these alloys further research might be accomplished to fully integrate γ-TiAl in future engines.

The most attractive property of γ-TiAl alloys is its high specific tensile and fatigue strengths at service temperatures. Nevertheless, its drawbacks concern their ductility and creep resistance. For these reason, in the last decades, the investigation of γ-TiAl alloys has been focused on enhancing the mechanical properties for structural applications at high temperatures by optimizing their microstructural design.

The objective of the present research work is to modify the microstructure and hardness of Ti45Al2Nb2Mn + 0.8(%vol)TiB_2 alloy by heat treatments. The evolution of the microstructure with respect to temperature is analysed through different techniques and the microconstituents and the phases involved are identified.

1. State of the Art

1.1. Intermetallics

Intermetallics are materials with ordered crystallographic structure. They are formed by two or more species of metal-metal or metal-semimetal strong bonding and they are characterized by near-stoichiometric composition. This specific structure gives them very different properties when they are compared with metals. [1, 2]

Intermetallic alloys have an ordered arrangement of mixed atoms which lead generally to materials with higher strength and lower ductility due to the restrictions that are imposed in the structure, as larger shear displacements are required to plastically deform the lattices [1, 2]. Intermetallics are attractive materials for structural applications. Examples of intermetallics are Ni_3Al, FeAl, TiAl or $MoSi_2$. According to Dimiduk at al. [3], only three classes of intermetallics have actually matured sufficiently to offer an emerging competitive balance of properties in the structural materials area: the $L1_2$ structured nickel aluminides, the B2 structured iron aluminides and the $L1_0$ structured gamma titanium aluminides.

1.2. γ-TiAl alloys

γ-TiAl intermetallics present low density (3.9 – 4.2 g/cm^3), high specific yield strength (figure 1), high specific stiffness, good oxidation resistance and good creep properties [4].

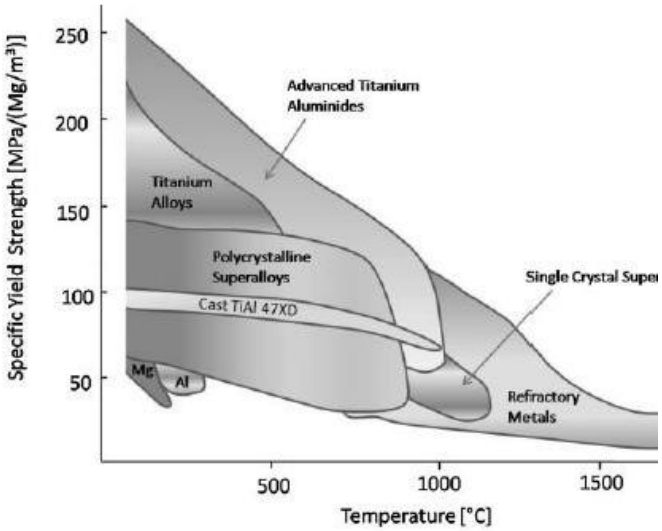

Figure 1: Variation of specific yield strength with temperature for structural alloys and selected intermetallics. [4]

There are numerous types of titanium aluminides which are being investigated depending on their composition. The main ones are referenced in table 1.

Alloy name	Composition (at%)	Alloy properties
General Electric, USA: 48-2-2	Ti-48Al-2Cr-2Nb	Ductility, fracture toughness and oxidation resistance
Plansee, Austria: γ-MET	Ti-45Al-(5-10)Nb	High temperature strength, creep, fatigue and oxidation resistance
GKSS Research Center, Germany: TNB Alloy	Ti-(45-47)Al-10Nb	High temperature strength, creep and oxidation resistance
Martin Marietta Laboratories, USA: XD™ TiAl	Ti-45Al-2Mn-2Nb-0.8B	Ductility, high temperature strength, stiffness, creep and oxidation resistance

Table 1: TiAl state of the art alloys by K.Kothari et al. [1]

γ-TiAl alloys for engineering applications are typically composed by intermediate Al concentrations (45 – 48%). Additions of other elements such as niobium and manganese improve ductility and high temperature capability, respectively [5]. These alloys are complex multi-phase alloys which can be processed by ingot casting or powder metallurgy routes. Depending on the processing conditions, specific microstructures are obtained which can be altered and optimized by thermo-mechanical processing or subsequent heat treatments. [4]

For this project the analysed material is Ti-45Al-2Nb-2Mn + 0.8vol%TiB_2 (Ti4522XD alloy). According to Rolls Royce in 1999, it is an established gamma alloy with the highest strength of those commercially available [7]. This alloy has competitively high specific tensile and fatigue strengths, good castability, but low creep resistance and fracture toughness. Its deficiencies in brittleness at low temperatures can be overcome by understanding their microstructure and modifying the design criteria [7]. D. Y. Seo et al. [7, 8] proved that creep strength could be improved by appropriate heat treatments. By aging a fully lamellar Ti-48Al-2W, the tensile strength at 760 °C was increased and the instantaneous creep strain reduced. In addition to this, several compositions with additions of W, Mo, Nb, Cr, or a combination of these elements have been developed to improve creep resistance [7].

There are numerous phases which can form the γ-TiAl alloy as it can be observed in figure 2. Particularly, at intermediate Al concentrations γ-TiAl alloys are composed by a minor volume fraction of α_2 (Ti_3Al) and a major volume fraction of γ (TiAl). These are the most relevant TiAl phases for engineering applications and they will be carefully described hereinafter.

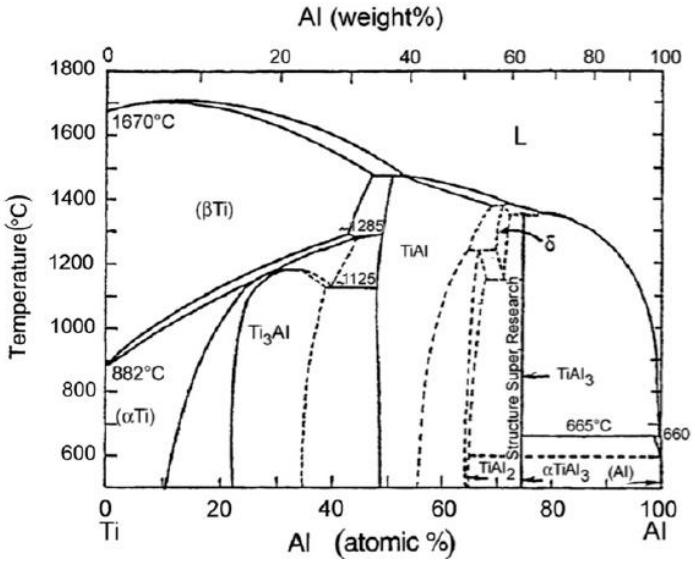

Figure 2: Ti-Al phase diagram [1]

The α_2 phase (Ti_3Al) results from the ordering reaction of α phase (disordered hexagonal phase of the A3 type structure) and corresponds to an ordered hexagonal closed packed (hcp) structure of the DO_{19} type (figure 3-a) [10, 11]. It exhibits good strength at high temperatures, although it has very low ductility. Moreover, high rate of oxygen and hydrogen absorption is found in α_2 phase producing its further embrittlement at high temperatures [1]. γ phase (TiAl) corresponds to a face centred tetragonal (fct) ordered phase of $L1_0$ type structure (figure 3-b) with a c/a ratio of approximately 1.02. This phase has been found to exhibit excellent oxidation resistance and it has very low hydrogen absorption [1]. The major plastic strain accommodation of γ-TiAl is carried out by γ (TiAl) phase [12, 13].

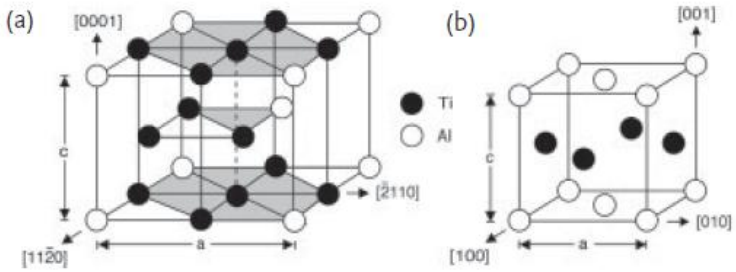

Figure 3: Crystal structures of binary Ti aluminides phases: (a) Hexagonal α_2 (Ti_3Al) phase and (b) tetragonal γ (TiAl) phase. [9]

Efforts have been done towards the refinement of the dual phase (α_2 + γ) microstructures by micro-alloying so as to enhance its properties [1].

1.3. γ-TiAl phase transformations

In two-phase TiAl based alloys three major transformation modes can occur: lamellar transformation, discontinuous coarsening and massive type transformations (formation of monolithic γ grains from α).

The most typical transformation in these alloys is the lamellar transformation. It occurs, as observed in the phase diagram of figures 2 and 5, either through transformation of α into (α + γ) and then (γ + α_2), or through the formation of α into α_2 and then (α_2 + γ). For 45 at.% Al compositions alloys this transformation implies the eutectoid reaction. The formation mechanisms of lamellar structures consist of a pre-nucleation stage where the crystal structure changes from hcp to fcc (face-centered cubic). Then, there is a nucleation and growing stage in which the equilibrium γ phase appears through both a chemical composition change by atom transfer and an ordering of the fcc zone. Finally, an ordering stage where the reaction of the fcc type structure leads to the final γ phase (fct). [10]

Discontinuous coarsening is a modification of the primary lamellar structure. It occurs depending on the alloy composition and the heat treatments. The transformation mechanism produces that both composition and volume fraction of the two phases (α/γ) attain equilibrium through the growth or coarsening of primary lamellae of a given grain at the expense of the adjacent [14].

Massive-type transformations occur basically during quenching although it depends also on the alloy composition. It involves a direct α → γ transformation. [14]

In addition to these transformations, during the cooling process, the cooling rate influences the final microstructure. In general, as the cooling rate increases, the microstructure changes in the following sequence: lamellar → γ_w + γ_M + lamellar → γ_w + γ_M → γ_M + α_2. Widmanstätten (γ_w) and massively transformed (γ_M) structures are said to be detrimental to mechanical properties [8]. According to D.Y. Seo et al. [8], the type of grain boundary that appears in the furnace cooling condition presents interlocked morphology. The formation of interlocked lamellar grain boundaries, as a result of slow cooling, is due to the higher α → lamellar transformation temperature and the larger driving forces for γ formation. Thick α_2 and discontinuous γ lamellae are often observed in furnace cooling [8].

1.4. γ-TiAl microstructure

Titanium aluminides can exhibit a wide variety of microstructures depending on the volume fraction of equiaxed grains and lamellar colonies. Lamellar colonies consist of stacked lamellae of α_2 and γ phases that form during the phase formation sequence α→ α + γ→ α_2 + γ at medium cooling rates. As it can be followed in figures 2 and 5, lamellae structure starts to precipitate in the two phase (α + γ) field. The α transform in an ordering reaction to α_2 at the eutectoid temperature at the same time that the equilibrium volume fraction of γ phase increases abruptly leading to the precipitation of γ lamellae. [15]

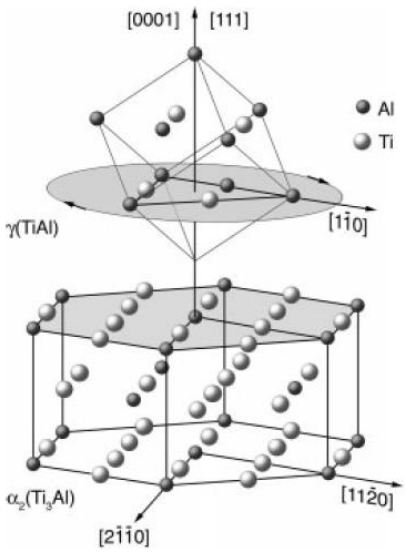

Figure 4: Crystallographic alignment of the α_2 (Ti_3Al) and γ (TiAl) platelets within the lamellar microstructure [15].

The lamellar microstructure contains interfaces between α_2 and γ phases, apart from differently oriented γ platelets (orientation variants). The closed-packed planes and directions matches into a particular orientation, shown in figure 4 and described by the Blackburn orientation relationship [15]:

$$\{111\}_\gamma \| (0001)_{\alpha_2} \; and \; < 1\bar{1}0]_\gamma \| < 11\bar{2}0 >_{\alpha_2}$$

γ-TiAl microstructures are classified into four types called near-gamma, duplex, nearly-lamellar and fully lamellar. Near γ consists of a microstructure formed by fully equiaxed grains, the duplex type is characterized by a microstructure where the equiaxed grains and the lamellar colonies are evenly distributed, nearly lamellar microstructure is called when the lamellar colonies are found in a greater proportion than equiaxed grains and finally, fully lamellar type consists of lamellar colonies all over the microstructure. The microstructures which have shown a wider range of commercial applications due to their balanced properties are the duplex and fully lamellar microstructure.

- Near gamma microstructures are obtained when the material is heat-treated in the (α_2 + γ) field, i.e. at a temperature near T_4 (figure 5). Coarsening of the existing γ grains is produced at this stage. It is characterized by a mixture of γ and α_2 grains as observed in figure 5. [1]

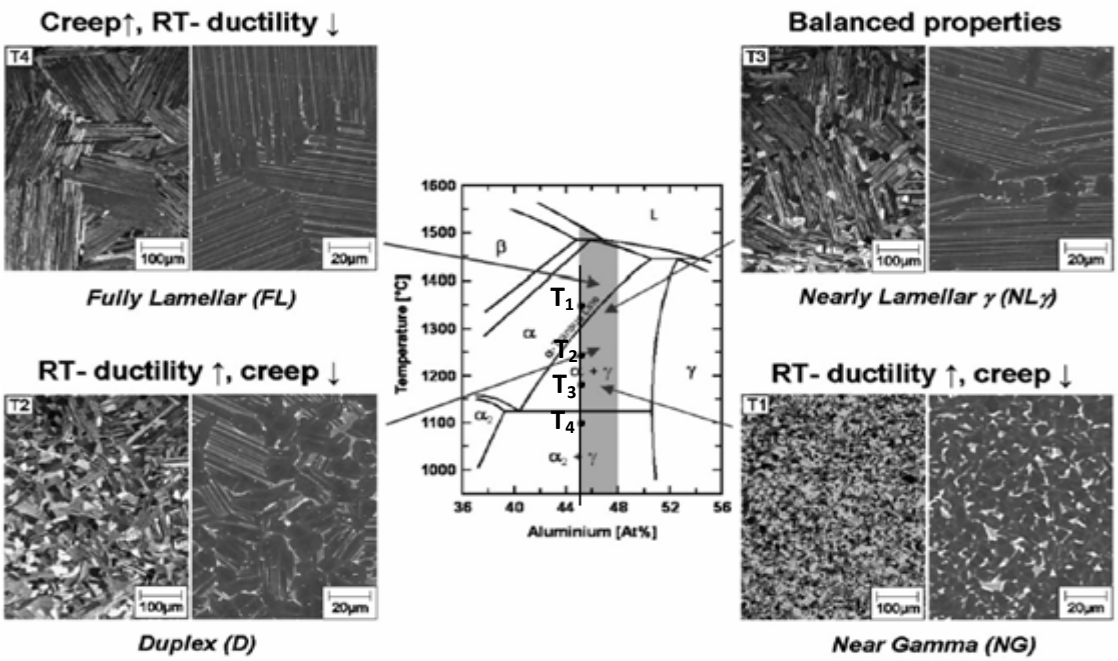

Figure 5: Mid-section of the binary Ti-Al phase diagram and representative microstructures obtained by means of heat treatments within the α and (α + γ) phase fields. γ-TiAl appears dark, whereas α_2-Ti_3Al shows a light contrast. [6]

- Duplex microstructure is found on samples subjected to heat treatments within the (α + γ) phase field near the eutectoid temperature. It corresponds to a temperature in which the α/γ volume ratio is close to 1. Due to the heat treatment the existing α_2 particles are dissociated. Additional α precipitates are nucleated to grow into α plates that leads together with γ plates to lamellar microstructure. In parallel, γ phase volume fraction is reduced until its equilibrium. Both phases tried to grow and limit each other, which finally resulted in a fine-grained structure. [1]

- Nearly lamellar microstructures are obtained at temperatures below T_α and above T_e in the (α + γ) domain. The process is similar to the duplex microstructure in which after reaching equilibrium due to a higher temperature in this case, more α phase grains

appear with its consequently associated coarsening that can be transformed to lamellar structure. Thus, this structure is characterized by coarser lamellar colonies and finer gamma grains. [1]

- When a heat treatment is done above the α-transus temperature the microstructure is characterized by higher volume fraction of large lamellar colonies that leads to a fully lamellar microstructure.

The previously discussed γ-TiAl microstructures are associated to specific processing or heat treatments temperatures (figure 5). They are obtained in four different regions according to the phase field boundary and also to other two important temperatures, the T_α temperature (α transus temperature) making reference to the boundary between α and (α + γ) phase fields, and the eutectoid temperature (T_e) where the eutectoid reaction is observed. According to Kothari [1] the eutectoid temperature is 1125 °C for a Ti-Al alloy. Nevertheless, with the introduction of other elements such as Nb, Mn and B, this temperature varies.

Therefore, the temperatures and ranges are not exactly represented in the phase diagram. They vary depending on the alloy composition and also on previous heat treatments. In the case of the work reported by D.Y. Seo et al. in [8] the transus α temperature was found to be 1310 °C for an investment cast Ti4522XD alloy whereas in [16] the measurements performed by C. Yang et al., it was at 1300 °C (10 °C lower) for the same alloy but HIP. In the thesis of R. Muñoz Moreno [17], it is reported that the T_e is 1150 °C, T_α is 1290 °C and the melting temperature is 1490 °C for the Ti4522XD centrifugal casting alloy determined by differential thermal analysis (DTA). The latter will be considered as a reference for the presented research work as the materials are the same.

D. Y. Seo et al. [8] reported that investment cast Ti4522XD alloys and heat treated at 1350 °C for 2 h results in a fully lamellar structure [8]. This microstructure is maintained as long as the specimen is above the transus temperature. Equiaxed grains start to appear when the samples are heat treated below 1310 °C (non straight lamellae appear). Domain boundaries are observed in the γ plates and the volume fraction of equiaxed γ grains increases as heat treatment temperature decreases. In this work done by D. Y. Seo et al. [8], it was concluded that γ thickness and α_2 thickness increases and lamellar volume fraction decreases as heat treatment temperature decreases, but grain size remains unchanged. Therefore, heat treatments after processing γ-TiAl are determinant in the final microstructure.

1.5. γ-TiAl mechanical behaviour

Regarding previous work done in the Ti4522XD alloy, the mechanical properties related to the types of microstructure are explained hereinafter.

- Decreasing the lamellar volume fraction reduces tensile strength while increasing the volume fraction of equiaxed grains promotes higher ductility values. [16]
- The process of ageing in as HIP powders does not introduce any difference for both near γ and near lamellar microstructures and consequently the tensile properties. [16]

- Near γ microstructures exhibit zero ductility in materials made by HIP at 1260 °C and by HIP plus heat treatment at 1010 °C, associated to its low fracture toughness and the presence of defects which acts as crack initiators (pores and coarsened borides). The enrichment of brittle α_2 grains in the prior particle boundaries may be also significant in reducing its ductility. [16]
- Fine near lamellar microstructures are obtained by HIP or heat treating above the α transus. It leads to high tensile strength values and a balanced ductility. Near lamellar microstructures exhibit comparable properties to usual cast and cast plus HIP alloys. [16]
- Investment cast TI4522XD alloys, shows that hardness values decrease gradually as the casting temperature decreases from 1400 °C (above T_α) to 1300 °C (below T_α) in a fully lamellar refined microstructure produced by oil quenching. It is related to the increase in lamellar spacing and the existence of more equiaxed γ grains. [8]

1.6. γ-TiAl alloy design

Improvement of creep and oxidation resistance of TiAl components has been achieved thanks to the alloy design and the corresponding microstructure tailoring. Nevertheless, there is not a unique microstructure with balanced properties. Each application has its requirements and the best way to fulfil them is to adapt and evaluate the alloy composition suitable for the specific designs.

Al concentration between 40 at% and 48.5 at% yields dual (α_2+γ) phase alloys. The ductility in this dual phase alloys is shown to increase with increasing Al concentration up to 48 at%. However, the ductility is highly influenced by the microstructure type and grain size that the thermo-mechanical processing has produced. [1]

Additions of elements involving Cr, V and Mn, lower the stacking fault energy and increase the propensity of twinning, i.e. deformation is more easily produced [1]. Although, as reported by F. Appel et at. [18], the exact influence and relation with ductility is not easily determined. Additions of alloying elements such as Nb, Ta, W and Mo increase the overall density and they are segregated within cast material. However, the main property and advantage is that they tend to increase the oxidation and creep resistance at high temperatures [1]. Furthermore, Nb and Mo are β-stabilizing elements that shift the T_α line to the Al-rich side narrowing the (α+γ) phase boundary. In other words, α and α_2 volume fraction is increased [4]. Finally, additions of B, C or Si are primarily used for grain refinement to produce lamellar microstructure with fine colony grain size (B) and to improve creep resistance (C, Si) [18]. Boron additions range from 0.1 to 1 at% and they avoid the growth of grains in the α phase field to form fully lamellar structures [1].

The dual phase (α_2+γ) TiAl is very sensitive to composition and small fractions of alloying elements works properly. Young-Won Kim classified a 1st generation of γ-TiAl based alloys exemplified by the composition Ti-48Al-1V-(0.1C) and defined by the first major programme initiated by the U.S. Air Force Materials Laboratory which at that moment (1975-1983) recommended this alloy composition in terms of ductility and creep resistance [19, 20].

Nevertheless, it did not fulfil the requirements for any engine component and, a second major development programme was again initiated in 1986 leading to the most common γ-TiAl based alloys. Their composition can be summarized as:

$$Ti_{45\text{-}52} - Al_{45\text{-}48} - X_{1\text{-}3} - Y_{2\text{-}5} - Z_{<1}$$

where, X = Cr, V, Mn; Y = Nb, Ta, Mo, W; and Z = C, B. Ti- 45Al-2Nb-2Mn + 0.8TiB_2 (Ti4522XD) alloys fall in this category and they are within the well-known 2nd generation of TiAl alloys. [1, 4]

In the 3rd generation of alloys the composition could be expressed as:

$$Ti_{52\text{-}58} - Al_{42\text{-}48} - X_{0\text{-}10} - Y_{0\text{-}3} - Z_{0\text{-}1} - RE_{0\text{-}0.5}$$

where, X = Cr, Mn, Nb, Ta; Y = Mo, W, Hf, Zr; and Z = C, B, Si. RE stands for rare earth elements. An example of these types of alloys is TNB alloys that are characterized by high Nb content and small additions of B and C [4]. They are high creep resistant alloys [4].

1.7. Processing of γ-TiAl alloys

The most popular manufacturing methods for the production of TiAl components are investment casting, ingot metallurgy (IM) and powder metallurgy (PM). Other advanced techniques still under research are laser forming or rapid sintering/consolidation processes such as spark plasma sintering [1]. The main processing problem is related to its cost. In order to obtain high performance parts it is necessary to subject the material to post-processing techniques. However, it has an important impact on the final value of the pieces. Therefore, it is very important to investigate and evaluate the alloying design, the microstructure and advanced near-net shaping manufacturing methods to achieve high efficiency levels. The processing techniques of the material studied are carefully described in the following sections.

1.7.1. Centrifugal Casting

The basis of centrifugal casting is the use of centrifugal forces applied to the moulds during solidification. In that way, constant pressure is exerted to the molten metal which results in high quality and integrity final components.

Investment casting has been during the last years the optimum method for the manufacturing of turbocharger turbine wheels. However, this process showed several drawbacks such as significantly prolonged high consumption of electricity, the heavy ceramic shell assembly, and severe environmental problem. Centrifugal casting is a recent technique which combines traditional die casting and gravity permanent mould die casting with major advantages as the elimination of porosity and shrinkage, good surface finish and good dimensional accuracy. [22]

In general, significant macro- and microsegregation is found in ingots and casting of TiAl alloys produced by skull melting. In centrifugal casting this problem is reduced as it is reported for the case of valves and thin blades [22]. Nevertheless, it is not eliminated and in thicker sections microsegregation can appear. Powder metallurgy provides an alternative way to produce a refined and homogeneous microstructure and can also manufacture near net

shaped components [16]. Another option is to do post processing techniques to solve the drawbacks. For example, investment cast bars can be hot isostatically pressed in order to eliminate cast porosity. [8]

1.7.2. Hot Isostatic Pressing of powder

Hot Isostatic Pressing (HIP) consists of the encapsulation of powder in a container with the suitable size and shape. It is sealed and isostatically compressed at elevated temperatures using inert high-pressure gas. The container is usually made from titanium or steel. The temperature range at which HIP is frequently carried out with TiAl alloys, goes from 1000 °C to 1300 °C under gas pressures of between 150 MPa and 200 MPa for 2 to 4 h periods [23]. These parameters are very important to the microstructure which will exhibit different behaviour according to the alloy composition and temperature range and, consequently, will have significant effect on the mechanical properties.

Regarding the phase distribution of these alloys according to F. Appel et at. [23], there is a lower volume fraction of α_2 in HIP materials and a higher γ volume fraction. Zhang et al. [23] explained that It might be because under high pressures, T_α may be increased or that the kinetics of the γ to α transformation are significantly slower compared to those under atmospheric pressure when the material is HIP. The presence of high volume fraction of γ has been assessed by Huang et al. [23] as a consequence from its lower atomic volume compared to the α_2 phase.

Some of the problems related to ingot metallurgy and casting such as center line porosity, chemical inhomogeneity, regions of varying density and microstructure can be mitigated or completely solved by powder metallurgy. In HIP of powders, the porosity in the final part is limited and the microstructure is homogeneous with little segregation. However, the drawback is that, due to the high temperatures required for the HIP treatment, the size of the grains increases and it is difficult to control the grain growth of the final part. [1]

The work of C. Yang et al. [16] study a Ti4522XD alloy HIP at 900, 1260 and 1350 °C and confirms that the properties obtained by HIP are comparable with those of near net shape casting processed samples. HIP at 900 °C gives rise to an equiaxed γ microstructure. At 1260°C, near γ microstructure is obtained with an increase in the fraction of α_2 grains in the prior particle boundaries. Moreover, the grain sizes along the boundaries are much larger than those inside. Finally, HIP at 1350 °C resulted in a near lamellar microstructure which is composed of lamellar colonies and equiaxed α_2/γ grains. Therefore, HIP at different temperatures and, hence in different phase fields, gives rise to different microstructures. In addition, it is reported that fine powders give rise to smaller lamellar colonies, but also to a smaller lamellar volume fraction. [16]

1.8. Applications

Titanium aluminide alloys are a promising future material for the aerospace field especially when new aircraft are sought to be more environmentally-friendly by burning less fuel and be quieter. The main advantages that offer this material over other alloys are that its weight is about a half of other conventional nickel alloys and that it can withstand high temperatures

without losing its properties. These properties present an excellent alternative to nickel alloys for the low pressure turbine (LPT) blades. However, it has also a major drawback. It has low ductility, in particular at room temperature, which complicates its machining. Nevertheless, this property can be enhanced by modifying the alloy composition and by microstructure tailoring. [24]

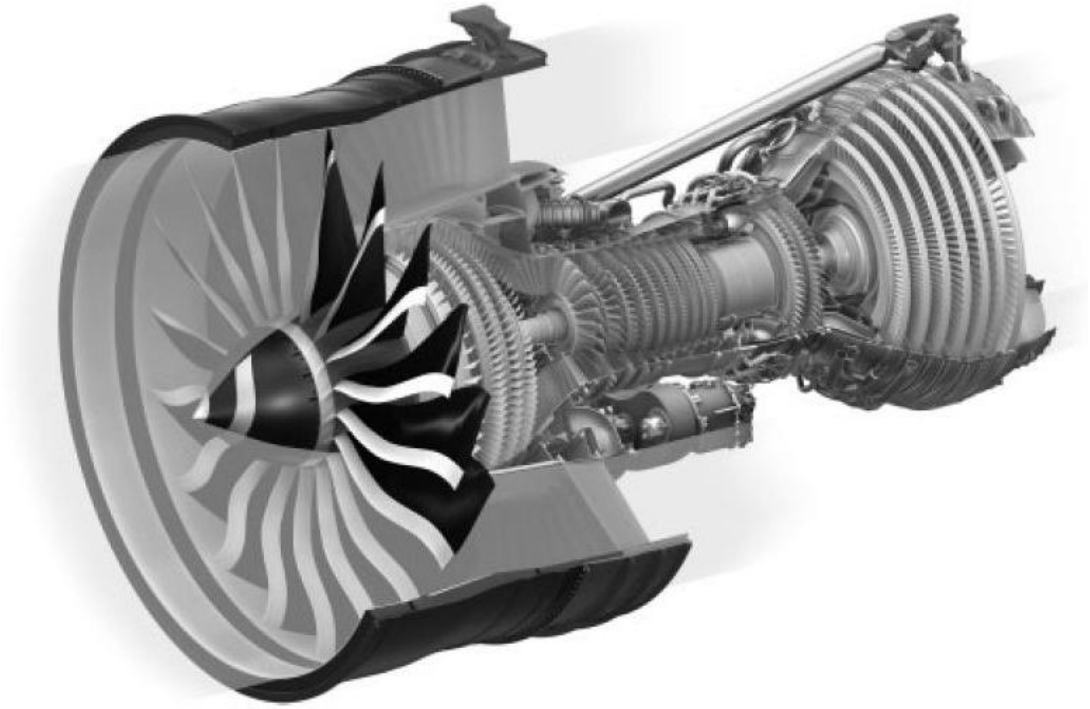

Figure 6: The General Electric GEnx-1B engine for the Boeing 787 Dreamliner. First real world engine to use TiAl. [26]

In 1999, an article published about the future use of gamma titanium aluminides by Rolls-Royce suggested that Ti-45-2-2-XD could only be used up to 650 °C where creep and oxidation resistance become an important aspect to be considered. Therefore, to overcome the difficulties in casting and machining and to improve its performance at high temperatures, the alloy composition was thought to be modified. Nevertheless, independently of the composition gamma titanium aluminides were said to have a high probability of being used in Rolls-Royce aero-engines in the near future, not only for LPT but also for combustor and turbine components reaching temperatures as high as 800 °C. [25]

Nowadays, General Electric (GE) has certified and implemented TiAl in the new GEnx-1B engine that powers the Boeing 787 Dreamliner which entered in service in 2011 (figure 6). The composition of this alloy is Ti48Al2Cr2Nb and is used in the last two stages of the LPT blades. [27]

Furthermore, MTU AeroEngines' design engineers have been working on the development of the Geared Turbofan™ (GTF™) engine, which will be soon powering the Airbus A320neo and other aircrafts. It is used in the blades of the high speed LP turbine. They are looking for the next step in high-temperature resistance with the fourth generation of titanium aluminides to further improve the future engines towards a more efficient and environmentally compatible design. [24]

However, in addition to blades, other components are being studied and tested including stator vanes, exhaust components, combustor casings, radial diffusers that control the deceleration of compressor charge gas into the combustor, transition duct beams and turbine-blade dampers (developed by Volvo). For example, vanes are used for low and high temperature operations leading to weight saving. The duct beam had shown good behaviour at high strain-rate loading. Finally, dampers achieve 50 % reduction of dynamic stress at low excitation frequencies [26]. There are investigations being performed for the use of gamma titanium aluminides in future supersonic high speed civil transport. Its mission is to reduce noise and exhaust pollution (as in subsonic aircraft engines). Some of the structures believed to be possible made of this alloy includes divergent flaps, nozzle sidewall and other structures at the back of the engine. TNB alloy (see table 1) was used to manufacture scramjet engine flap subelements by GKSS. [26]

However, in addition to the usual aircraft engine applications, there are other uses that have become important. The automotive and the naval industry are examples of them.

As in the case of aerospace field, fuel consumption improvement and emissions reduction are major concerns for the automotive industry with the increasing enforced legislation in Europe and USA. Lightweight high temperature resistant components such as engine valves, turbochargers wheels and connection rods are required for internal combustion petrol (up to 1050 °C) or diesel engines (up to 850 °C). Additionally, efficiency and performance of these engines will be enhanced in this high temperatures range leading to a rise in gas pressure and engine revolutions per minute. Here is where the gamma titanium aluminides play a fundamental role that brings this sector to the second most important application. TiAl can replace exhaust valves of steels and Nickel-based superalloys and regarding the intake valves the speed of the engine could also be improved. One of the problems of the valve material is that wear requirements would not be fulfilled by its own. Research is being done in coatings that could solve this problem.

One of its applications was in Formula 1, although its use was banned in 2006. The material and mostly the machining and treatments involved are still really expensive. However, according to Gebauer [26] TiAl valves are almost ready for introduction and a cost-effective process for commercial mass production exists.

Turbocharger wheel material in diesel engines (figure 7) is another application that is being currently assessed and tested. Its benefits go from a reduction of emissions to an increase in the agility of the vehicle's responsiveness and in the maximum rpm of the turbine rotor leading to higher engine efficiency. Since 1999, when the first commercial application was announced, Mitsubishi, for example, has implemented TiAl turbocharger wheels in their Lancer Evolution 6 sports car. Furthermore, the progress in the application of this material could be extended to other industry areas such as ship engines (it has already been proved in a ferry). [4, 26]

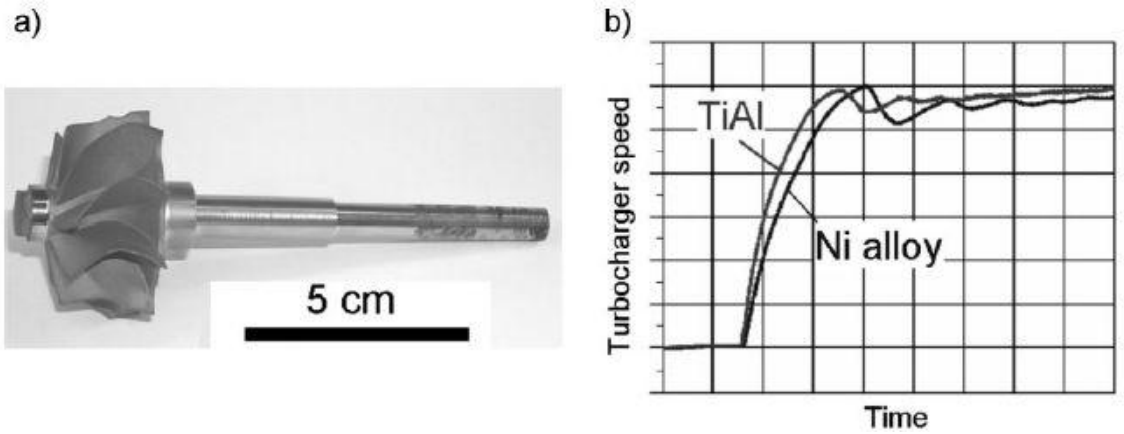

Figure 7: a) Turbine rotor with a TiAl wheel used for a diesel engine; b) result of a vehicle test with a car equipped with a TiAl turbocharger (XD45 alloy) and a conventional Ni-based turbocharger. [4]

To sum up, it could be said that a certain future for TiAl alloys exists in the aerospace field. Nevertheless, the same cannot be stated for the case of automotive industry where according to the authors of [26] greener alternative modes of power for ground transport, such as hydrogen/alcohol power fuel cells and battery-driven engines are demanded.

2. Experimental Procedure

2.1. Material and processing

The γ-TiAl intermetallic alloy used to carry out this bachelor thesis has been the alloy Ti-45Al-2Nb-2Mn (at%) -0.8vol%TiB_2 (Ti4522XD). This material was processed by centrifugal casting (CC) and powder metallurgy, in particular by hot isostactic pressing (HIP).

Centrifugal casting (figure 8) was carried out at ACCESS e.V. TechCenter (Aachen, Germany) in a Linn Supercast equipment with the following characteristics: mould rotation velocity of 250 rpm, mould preheating temperature of 1200 °C, superheat from 20 to 100 °C and with a ceramic mould coated with Y_2O_3. Then it was HIP to eliminate porosity. HIP was performed up to a dwell temperature of 1185 °C. [17]

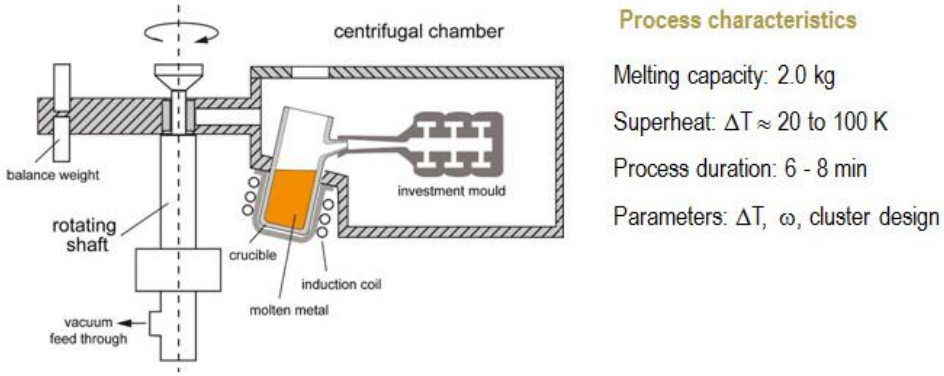

Figure 8: Investment casting of TiAl-based alloys: horizontal centrifugal casting LINN, provided by ACCESS e.V. TechCenter.

The HIP material was obtained from hot isostatic pressing gas atomized prealloyed podwers produced by EIGA (Electrode induction Gas Atomization) in the Helmholtz-Zentrüm für Material and Küstenforschung GmbH (Geesthacht, Germany). HIP conditions were: 1200 °C and 200 MPa for 4 hours at Forschungzentrum Jülich (Jülich, Germany). [17]

Heat treatments were carried out in a vacuum furnace Edwards High Vacuum International. As it was previously mentioned, the Ti4522XD alloy was modified to four different microstructures by heating up to four temperatures (figure 9): 1100 °C, 1190 °C, 1250 °C and 1350 °C.

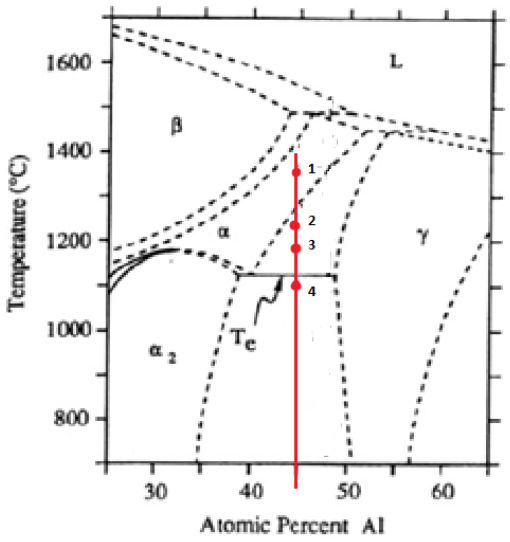

Figure 9: Phase diagram showing the four heat treatment's temperatures: 1) 1350 °C, 2) 1250 °C, 3) 1190 °C and 4) 1100 °C.

These temperatures were chosen according to the defined phase transformation temperatures (T_α = 1290 °C) and the eutectoid temperature (T_e = 1150 °C). Then, samples were furnace cooled (FC) to room temperature. The heating rate was 5 °C/min and the dwell was maintained during 2 h (figure 10). The samples were placed in a ceramic recipient with zirconia balls to avoid any contact between the materials.

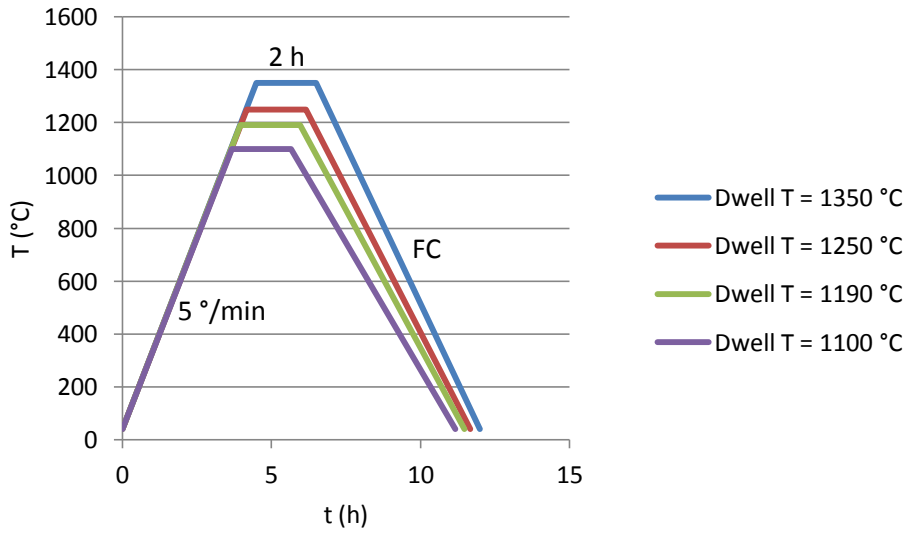

Figure 10: Scheme of the cycle followed in the vacuum furnace.

2.2.Microstructural characterization

CC and HIP samples were cut with a cutting machine MECATOME T201 A and a Struers Minitorm. The cut was always done with a lubricant favouring the cut and the material disposal. Afterwards, the pieces were cleaned with pressure water and ethanol and dried before the next step.

In order to manage the samples in subsequent activities, they were mounted with bakelite in a hot mounting machine Bitech Europe EP series.

Samples were metallographically prepared for posterior microstructural scanning characterization. Firstly, the samples were roughed down by an automatically rotating grinding machine Presi Mecapol p 320. The rotation velocity of the disk was 200 rpm and the lubricant used was water. Four different sandpapers with numerations of 180, 320, 600 and 1000 were used. The process is the following: the sample is hold in one direction until the lines appear all in the same direction. Then, the sample is rotated 90° and the striped pattern is drawn in that direction. When the lines appear very quickly in the same direction the sandpaper is changed to one of higher numeration. Furthermore, the optical microscope was used to observe the surfaces of the pieces to assure the final state. The samples that had been treated to higher temperatures were tougher; hence, the roughing down of the piece was done applying force manually. Once all the sandpapers were used and the surface was properly grinded, the polishing method was developed.

Polishing was performed at the IMDEA Materials Institute. An automatic polishing machine Buehler Metaserv™ 250 was used with four polishing cloths. The first three polishing cloths were used applying mono crystalline diamond paste of 9 µm, 3 µm and 1 µm, respectively. For this cloths, the lubricant was DP-Lubricant blue (alcohol-based lubricant). The parameters of the polishing were a minimum time of 15 min (repeated several times with the first cloth), the force application mode was from the piston and 20 N, the direction between the rotating plate and the rotating support of the pieces was opposite, and the rotation velocity was approximately 200 rpm. Final polishing was done with a colloidal silica suspension lubricated with water. This last step is very important and the time in this case was programmed in intervals of minimum 30 minutes. Between each sandpaper and polishing cloth, the samples were cleaned with water and ethanol, followed by a quick dry to avoid possible contamination. In addition to this, careful was taken in the managing of the cloths to avoid contamination between them.

Two chemical attacks were used to reveal the microstructure of some of the samples. It was necessary for the cases were the lamellar structure was not sufficiently formed or was inexistent. That is, for the HIP samples except for the one heat treated at 1350 °C. The etching was performed first by Kroll's reagent and then, by Keller's reagent. The reason for using two reagents was to obtain the best possible microstructural analysis and to be able to identify the modifications with heat treated temperatures at high magnifications.

Kroll's and Keller's reagent were prepared under a laboratory fume cabinet and taking the proper safety measurements. Kroll's reagent was made from 100 ml of water, 1-3 ml hydrofluoric acid and 2-6 ml nitric acid. The samples were immersed in the reagent solution for 3 seconds and then rapidly immersed in a recipient with water followed by a clean under pressure water. Occasionally, the samples were overetched but the images allowed distinguishing between the γ and α_2 equiaxed grains to measure the grain size. Keller's reagent was composed with 2 ml of HF, 3 ml of HCl, 5ml of HNO_3 and 190 ml of distilled water. The

samples were submerged this time for 1 second and the results were very similar to the previous case.

Despite the short time of the reaction, it was not efficient in revealing a better microstructure giving to overetching almost in all cases. Therefore, a final polishing of the samples with colloidal silica for about an hour was carried out. The dispersing and chemical mechanical polishing action allowed better quality microstructures [28].

Optical microscope (OM), scanning electron microscope (SEM) and atomic force microscope (AFM) were used to characterize microstructures which were later analysed by different image processing.

2.2.1. Scanning Electron Microscopy (SEM)

In an optical microscope light is its basic element. Ti4522XD samples are opaque at visible light. Consequently, only the surface can be observed by reflection of the light. With this instrument, the contrast of the image is achieved by differences in the reflectivity of the phases in the microstructure. The upper limit to the magnification with an optical microscope is approximately 2000x [29]. Therefore, although OM was used as a tool during the polishing process and in the measurement of hardness, it did not allow obtaining information about the microstructural features. In order to extract images to be later analysed with high magnifications, electron microscopy was used. This technique uses beams of electrons instead of light radiation. Once they are accelerated across large voltages, electrons can have wavelengths on the order of 0.003 nm. These short wavelengths allow high resolving and magnification power of electron microscopes. Transmission as well as reflection beam modes operation are possible for these microscopes (TEM and SEM, respectively) [29]. In this project scanning electron microscopy (reflection beam mode microscope) was used.

Scanning electron microscopy (SEM) is a technique that allows revealing information about a solid specimen (hard and soft, structural, functional and biological materials) [30]. The main characteristic of these microscopes is that by this technique it is scanned the sample applying low to medium energy through an electron beam focused over its surface [29]. Afterwards, the reflected beam is collected by a detector [29, 31]. The surface must be electrically conductive to allow this phenomenon. According to the interaction between the electron beam and the material, different types of signals are generated [32, 33]: secondary electrons (SE), backscattered electrons (BSE), energy-dispersive X-ray spectroscopy (EDS) and electron backscattered diffraction (EBSD). This last one is capable of analysing the crystalline structures and crystal orientations but it was unavailable for this project. The secondary electrons are used to obtain a topological image of the material. The BSE depend on the number of atoms of the sample and their atomic weight, producing a larger number of BSE in the signal the ones having larger atomic numbers. It allows differentiating between the contrasts provided by the different composition of the phases. These images allow measuring the size of the grains and colonies of the microstructures. Finally, EDS issued by the material is collected by EDS detector integrated in the SEM. It can be useful to make a semi quantitative chemical microanalysis through wavelength dispersive spectrometry. The electron coming from the electron beam

excites the atoms of the samples with the subsequent issue of X-rays. These X-rays are separated into an energy spectrum that by analysing its wavelengths and intensities, the elements can be identified as well as their concentration.

The microscope used in the experiment was a Philips XL-30 SEM at the UC3M laboratories. Moreover, the samples were subjected to energy between 15 to 20 kV and magnified in a range from 500x to 1-6.5kx in order to observe all the details. SE, BSE and EDS are the types of signals that were used to characterize the material.

2.2.2. Atomic Force Microscopy (AFM)

In AFM, also called Scanning Force Microscope (SFM) [34], short-range forces between a tip and the sample allow the sample topography to be recorded. Furthermore, it can simultaneously probe the mechanical properties of the surface by dynamically oscillating the cantilever that supports the tip [35]. Since its invention in 1986 by Binning and Rohrer [34], its application in life science has been determinant for imaging molecular and cellular specimens under different environments. AFM allows imaging in combination with locally probing functions of macromolecular elements. Its contribution to life science lies in the possibility of direct measurement of the samples without coating (electrically nonconductive samples can be measured directly). [35]

It consists of a sharp stylus that scans the surface of a sample by the approaching of the tip over the surface of the specimen [36]. Its topology is, therefore, traced and recorded. Usually, the stylus is located at the free end of a cantilever spring. When there is an elevation the tip moves up and the cantilever is bent upwards whereas when there is a depression the lever is moved down. Most stylus and cantilever are usually microfabricated from silicon or silicon nitride. In the present case, the tip was made from Sb doped with Si. The softer the specimen the softer the cantilever spring should be in order to trace the sample instead of deforming it. Deflection of the cantilever is measured to draw the sample topology. A laser beam is focused onto the back of the free end of the cantilever and it is then reflected off onto a four segment photodiode (figure 11). During the set-up of the microscope, the laser is aligned so that all four segments are equally illuminated. If the loaded tip bends upwards or downwards, the laser beam illuminates the two upper or bottom segments more strongly, respectively. The original deflection is then restored by a feedback loop. The position of the scanner with respect to the stylus is recorded and used as the AFM topographical image. [35, 36]

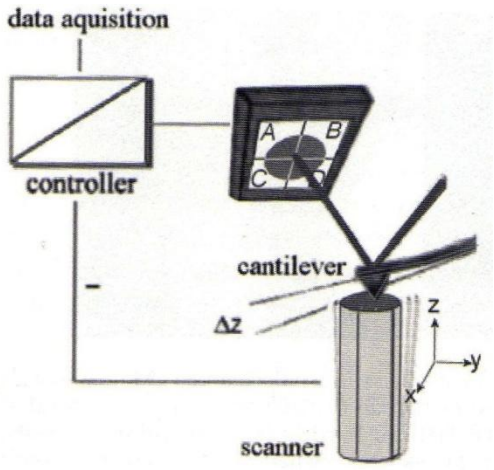

Figure 11: Elements of an AFM [35]

In dynamic AFM modes, the cantilever is oscillated and the amplitude and phase of the oscillation are monitored using the laser signal in the photodiode.

The interaction between the tip and the sample needs to be taken into consideration because it influences the results. Its advantages and drawbacks are listed in table 2. The stylus, most of the time, is loaded onto the sample by either intermittently (intermittent contact or tapping mode) or constantly (contact mode). It depends on the desired loading force that is achieved by approaching the probe and the sample and bending the cantilever.

Imaging Mode	Advantages	Disadvantages
Contact Mode	- High scan speeds - Only AFM technique that can obtain atomic resolution images - Rough samples with extreme changes in vertical topography can sometimes be scanned more easily in this mode	- Lateral (shear) forces can distort features in the image - The forces normal to the tip-sample interaction can be high in air due to capillary forces from the absorbed fluid layer on the sample surface - The combination of lateral forces and high normal forces can result in reduced spatial resolution and may damage soft samples (i.e. biological samples, polymers, silicon) due to scraping between the tip and the sample
Tapping Mode	- Higher lateral resolution on most samples (1 nm to 5 nm) - Lower forces and less damage to soft samples imaged in air - Lateral forces are virtually eliminated, so there is no scrapping	- Slightly slower scan speed than contact mode
Non-contact Mode	- No force exerted on the sample	- Lower lateral resolution, limited by the tip-sample separation - Slower scan speed than tapping and

Imaging Mode	Advantages	Disadvantages
		contact mode to avoid contacting the adsorbed fluid layer which results in the tip getting stuck - Non-contact usually only works on extremely hydrophobic samples, where the adsorbed fluid layer is at a minimum. If the fluid layer is too thick, the tip becomes trapped in the adsorbed fluid layer causing unstable feedback and scraping of the samples

Table 2: Advantages and drawbacks of the different imaging modes [34]

Microstructural and micromechanical characterization of TiAl alloys using AFM has been reported by S. Gebhard et al. [37] as an alternative to TEM and SEM. In this project the samples heat treated at 1350°C were analysed by AFM.

In the case of the AFM of UC3M laboratories (Digital Instruments Nanoscope™ Scanning Probe Microscope), the specimen is measured using an optical point. AFM was performed in the tapping mode. The characteristics of the tip besides its material (Sb doped with Si) were that it had force constant between 20-80 N·m with a drive frequency of 261.9 KHz.

Samples needed to be adjusted to the size allowed by the AFM, 10x10x3 mm. Therefore, they were cut and polished again. Moreover, they were attacked with Keller's reagent with a cotton bud to favour the revealing of the microstructure. With the images obtained, the lamellar spacing was measured.

2.2.3. Image analysis

Analysis software (Olympus Microscopes software) was used to determine different measurements regarding the microstructure [38]. This software allows calculating the grain size by drawing the boundaries of the grains and colonies through a polygon (figure 12). The programme calculates by the intercept method characteristics such as the mean diameter, the area or the perimeter, among others.

For each heat treatment temperature, a minimum of approximately 30 measurements were taken. Two types of microstructural features were considered: the colonies and the equiaxed grains. The number of measurements was determined by the lowest number that was available of the different features and taking into consideration that it must be an odd number. In the case of the colonies for the lowest heat treatment temperature of the HIP material, in particular at 1250 °C and 1190 °C, the number of measurements was 11 because not enough lamellar colonies were found due to their specific microstructure that will be explained later. For the HIP material treated at 1100 °C and the as HIP raw material before any heat treatment, no colonies were present in the samples and therefore, no measurements were carried out. Nevertheless, 27 measurements were taken into account to determine the grain size for the rest of the CC and HIP samples.

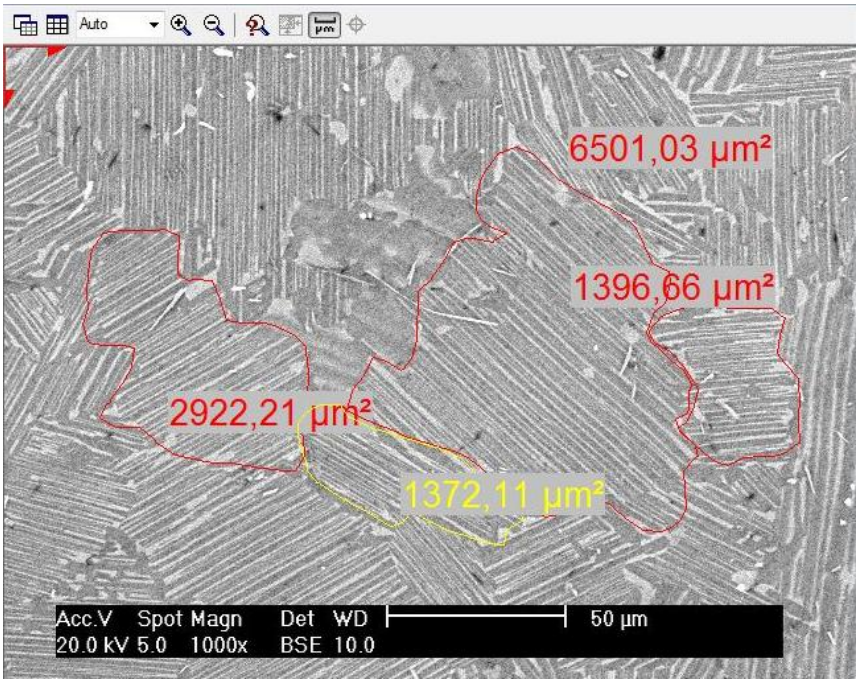

Figure 12: Example of colony size computation by analySIS auto.

In order to determine the microstructural evolution during heat treatment of the Ti4522XD alloy in terms of the phases and their distribution present at the different temperatures, the software ImageJ was used [39]. By providing to the computer the scale in which the images were taken at the microscopes, it is able to determine, among other possibilities, for example the area and its fraction of a specific phase. Through the image, which is usually transformed to grey levels, and by adjusting the threshold of the colours, it can compute the percentage of the image with the same range of colours. In our case, it was done manually, dividing the colours into: brighter white, light grey and darker grey pixels so that three group of microstructural features could be discriminated (α_2, γ and borides). By moving the threshold to these levels of grey, the phase could be selected and the fraction determined (figure 13). It was performed adjusting the limit of threshold with 5 images (the maximum available with high quality) of each temperature for both types raw materials (HIP and CC) and then, calculating the mean value.

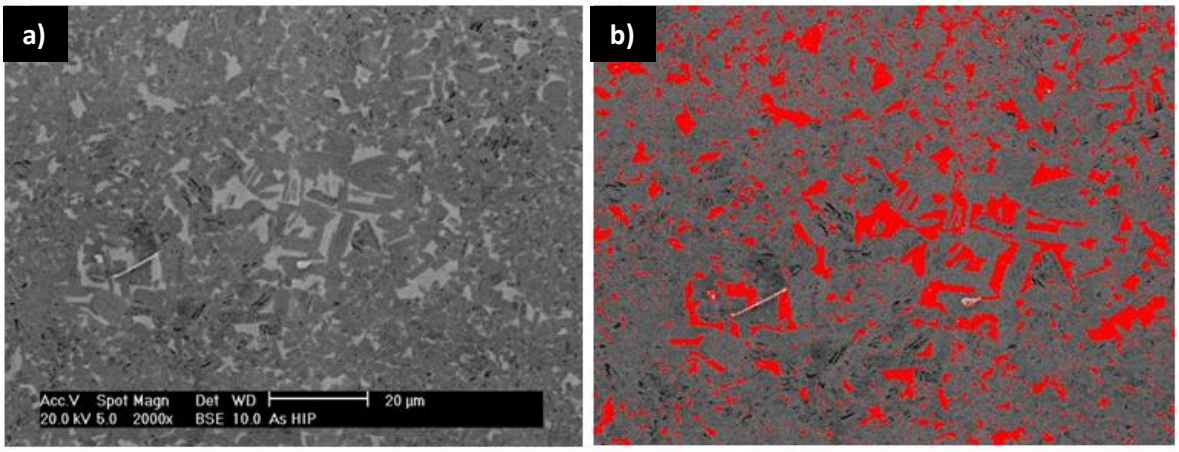

Figure 13: Comparison between a) original image of an as HIP sample b) determination of the α_2 percentage in imageJ of a).

2.3. Hardness characterization

Hardness measures the material resistance to plastic deformation [40] and, in many different materials it can be correlated with the ultimate tensile strength. There are numerous quantitative techniques that have been developed to measure hardness or microhardness. They are based on indentation over the surface of the tested material with a known load and velocity for the applied force. Afterwards, the print left by the indenter is measured according to depth or size in order to classify the material. In this project the test used to compare the hardness of the different samples of TiAl has been the Vickers Microhardness Test, sometimes also called diamond pyramid. As its name may suggest, the small indenter is made from diamond and it has a pyramidal shape. It is forced into the surface of the material with smaller loads than other hardness test, between 1 and 1000 g. The print produced by the indenter is then measured by an optical microscope in which the diagonals of the rhomboidal form are used to calculate the hardness number (figure 14).

This hardness number is designated by HV and it is computed with formula 1 in which the load applied, P, is in kg and the diameter, d_1, in mm. This test is useful to measure small regions of a sample without completely destroying it and it is also useful for fragile materials.

Figure 14: Side and top view of the indenter in Vickers microhardness test [40].

$$HV = \frac{1.854 \cdot P}{d_1^2} \qquad [1]$$

Hardness is dependent on size and orientation of the microstructure and the depth of penetration that could not be entirely taken into consideration in the experiment.

The size and the average diameter of the grains in a polycrystalline metal have a strong influence on its mechanical properties. However, the crystallographic orientations of adjacent grains and the grains boundaries that are consequently distinguished can trigger slip or dislocation motion during plastic deformation. These constitute then an important parameter affecting the mechanical properties of the material.

As the crystallographic misorientation of the grains and the atomic disorder within a grain boundary region increase, the dislocation motion is obstructed.

Therefore, fine grain size material is harder and stronger than one that is coarse grained [30]. For many materials including TiAl alloys the yield strength σ_y varies with grain size according to the following equation known as Hall-Petch relation [37, 41, 42]:

$$\sigma_y = \sigma_0 + k_y d^{-1/2} \qquad [2]$$

σ_0 is a stress contribution independent of grain size, k_y measures the difficulty with which slip penetrates from one grain to the next and d is the average diameter. The relation explains that the yield strength increases monotonically with decreasing the average grain size. However, when the grain size is reduced to the submicrometer range, k_y tends to decrease and when it is lower than 100 nm, k_y becomes negative. This is called the inverse Hall-Petch relation.

Microhardness Vickers Test was performed at the IMDEA Material Institute. In the study of the microhardness of the Ti4522XD, the load applied was 9.801 N, designated as HV_1, during 10 s. Differences appeared between measurements when the indentation was apparently being performed in the same type of surface. In the case of the HIP samples, as the grain size is much smaller than the indenter, the exact location where the indenter is doing the test could not be defined. Nevertheless, for the case of the CC pieces, two types of indentation where distinguished: inside the lamellar colony and other category group that encompasses both the indentation falling in the equiaxed grains regions and also one covering several colonies. In figure 15, Vickers test can be observed for the three cases.

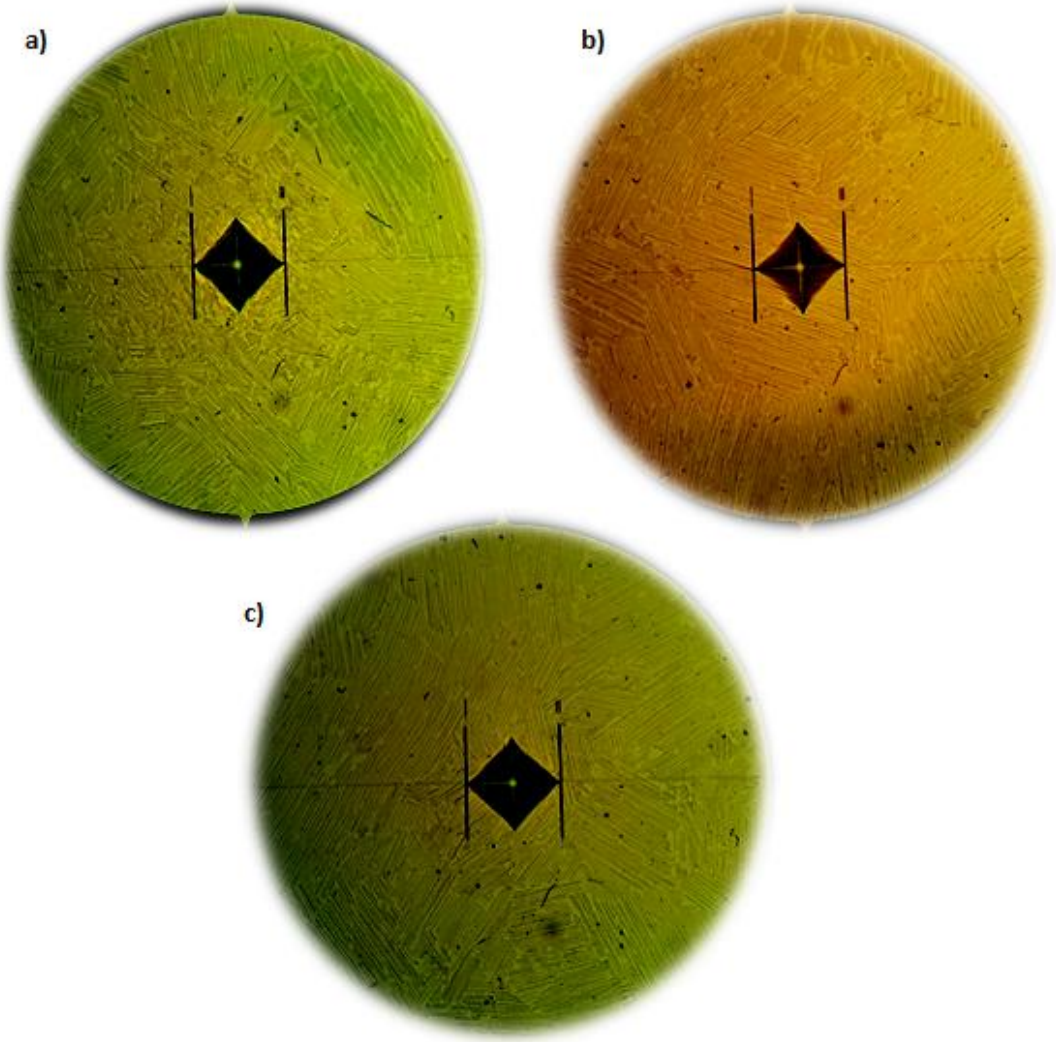

Figure 15: Microhardness Vickers Test in a) equiaxed grains with 307 HV_1, b) lamellar colony with 337 HV_1 and c) across different boundaries with 351 HV_1 in a CC sample heat treated at 1190 °C.

In the case of the HIP samples, at least 13 measurements were done for each microstructure (according to the heat treatments temperatures). For the CC samples, at least 11 measurements were performed for the centre of a colony and another 11 measurements at least were taken for the indenter falling outside the centre.

3. Results and Discussion

3.1. Microstructure characterization

3.1.1. SEM

Electron disperse scatter (EDS) was carried out in representative samples to identify the phases. EDS determined the proportion of the elements and confirmed that darker grains corresponded to γ phase and lighter grey grains to α_2 grains. The proportion encountered in the analysis agrees to the composition, approximately 50 – 50 % of Ti and Al in the γ phase and a ratio of 1/3 corresponding to the α_2 phase (Ti_3Al). In figure 16-a, the phases are identified. Finally, the EDS confirmed that the brightest shapes are associated to borides.

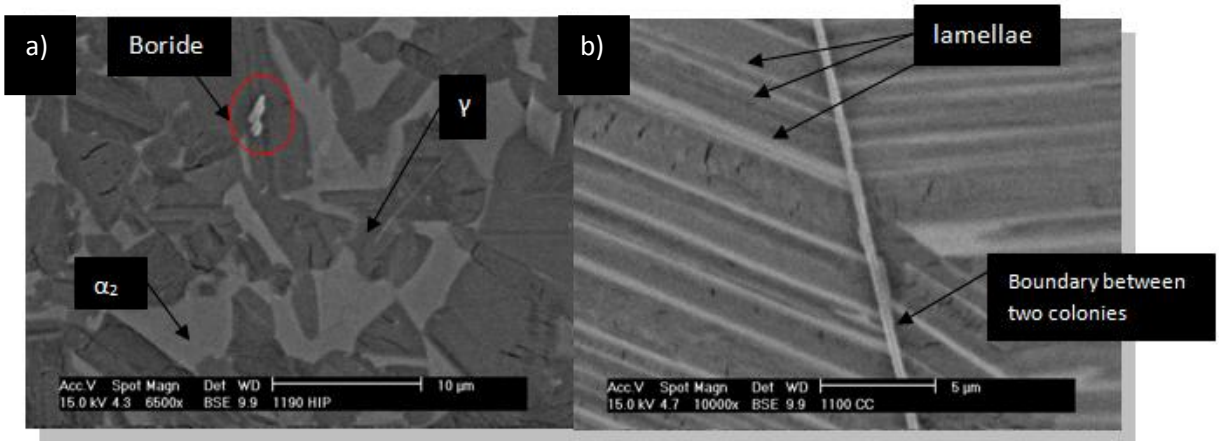

Figure 16: Characterization of a HIP sample at a) 1190°C and b) a CC sample at 1100°C.

In figure 16-b, the border in between two lamellar structures is found. It was also analysed by EDS and corresponds to Ti. The lamellae are marked to show the alternation between the two phases. It can be appreciated in the picture that sometimes there can be lamellae of the same phase oriented in different crystallographic variants and it is observed as a single lamella. The microscope did not allow us to distinguish individual lamellar variants and therefore, to calculate the lamellar spacing.

CC SEM microstructure

SEM micrographs of the CC material are presented in figure 17. CC samples show lamellar colonies at all treated temperatures. These lamellar colonies are characterized in these samples by interlocked boundaries. They are produced by the incursion of lamellae in neighbouring colonies (figures 17-a,b,c,e). Borides are presented in a globular shape in the different samples.

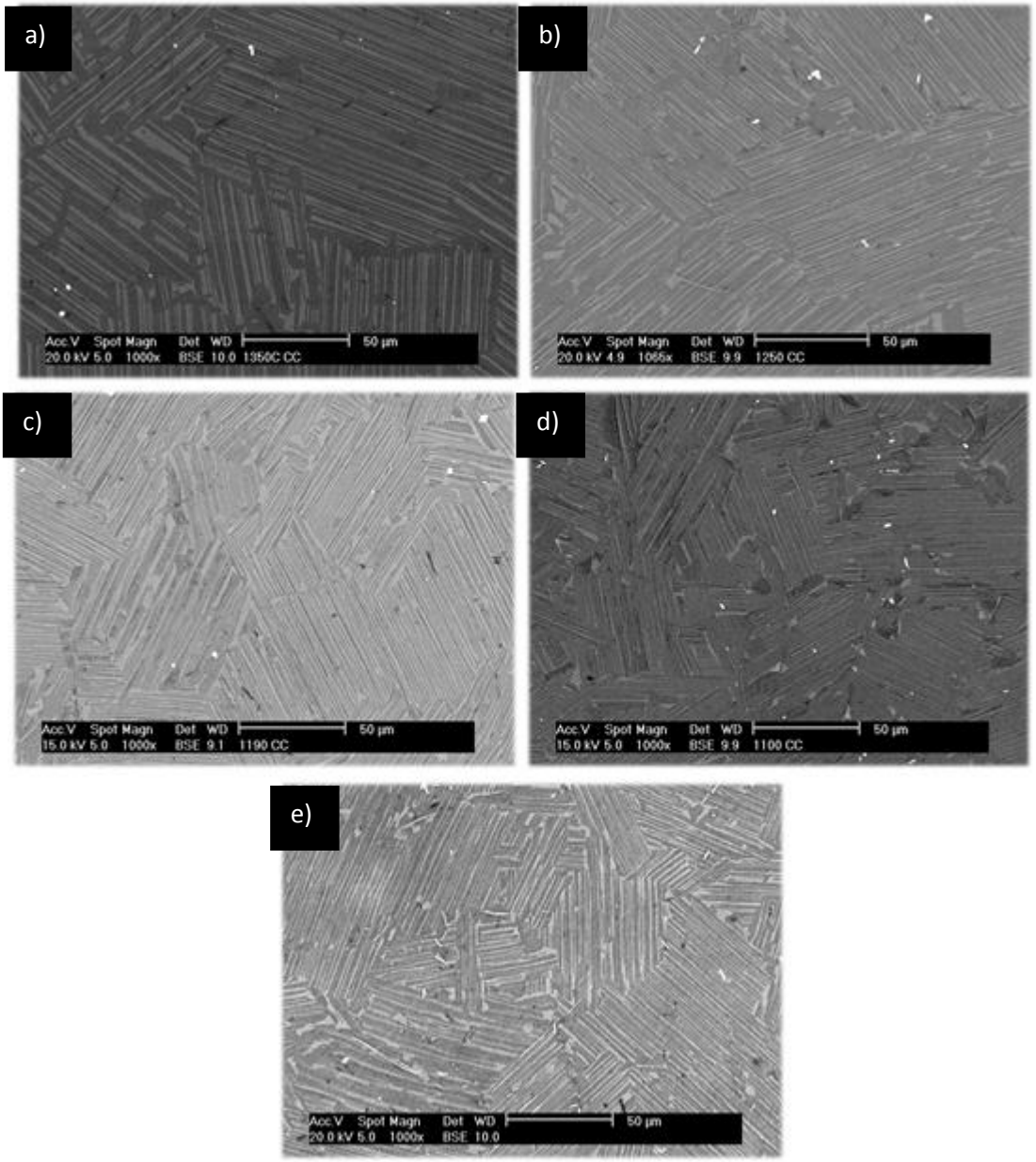

Figure 17: Images of the CC samples taken from the SEM at 1000x, heat treated at a) 1350 °C, b) 1250 °C, c) 1190°C, d) 1100 °C and e) as CC

The microstructure of the as CC (figure 17-e), CC-1100 °C (figure 17-d) and the CC-1190 °C (figure 17-c) materials are very similar, because the former was processed at 1185 °C and the other two are near the eutectoid temperature. T_α has not been crossed so as to promote more lamellar transformation. At 1100 °C with CC, the titanium is observed to diffuse to the boundaries of the lamellar colonies in figures 16-b and 18. In addition, in that figure 18 the globular shaped borides are identified. These three microstructures (as CC, 1100 °C and 1190 °C) could be considered nearly lamellar because there are regions in the surface where the grains become very numerous. Volume fraction of equiaxed γ grains decreases as heat treatment temperature increases and they start to disappear above 1250 °C, which is in accordance also with what D.Y. Seo et al. [8] reported.

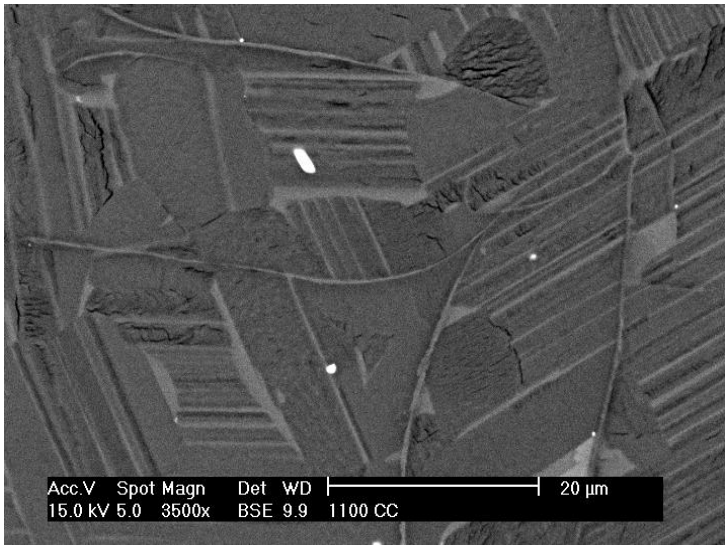

Figure 18: Image of the CC sample taken from the SEM at 3500x, heat treated at 1100 °C

For a heat treatment of 1250 °C (figure 17-b), despite not having crossed the T_α, there was enough α to be transformed into lamellae. Nevertheless, few equiaxed grains appear too but in a very small quantity better appreciated in figure 19. This is a fully lamellar microstructure.

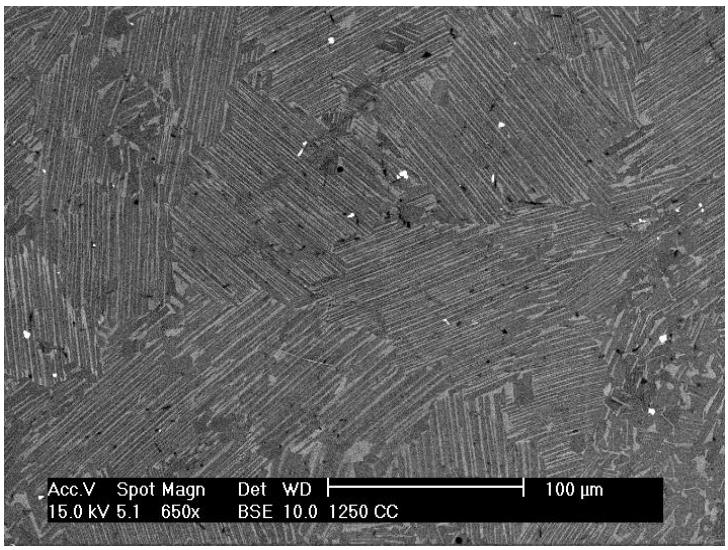

Figure 19: Image of the CC sample taken from the SEM at 650x, heat treated at 1250 °C

Near gamma and duplex microstructures are not observed in this processed material. The results of the CC specimens are similar to what was reported in [17] by R. Muñoz Moreno. At 1300 °C for 2 h, the microstructure is fully lamellar whereas in the as CC sample the microstructure is considered nearly lamellar. Finally, at 1350 °C (figures 17-a and 20), the T_α was crossed with high margin allowing having a fully lamellar microstructure in agreement with the work presented by D.Y. Seo et al. [8] in which it is stated that fully lamellar structures in XD alloys can be produced by supertransus heat treatments. In the CC sample at 1350 °C, lamellae are well observed in figure 20 to grow inside adjacent ones (interlocked boundary).

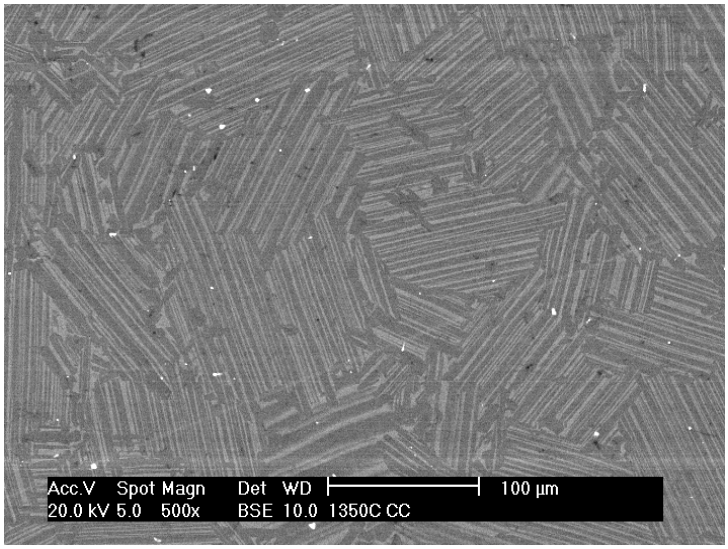

Figure 20: Image of the CC sample taken from the SEM at 600x, heat treated at 1350 °C

HIP SEM microstructure

In figure 21, the microstructure of HIP samples seems to be very different from the CC. The grains are much finer and the lamellae are limited. Borides in the HIP samples are less numerous and with a more needle shape in comparison to what was seen in the CC microstructures. Furthermore, small cracks are shown in following figures in the γ phase at high magnifications that were not observed in the CC samples.

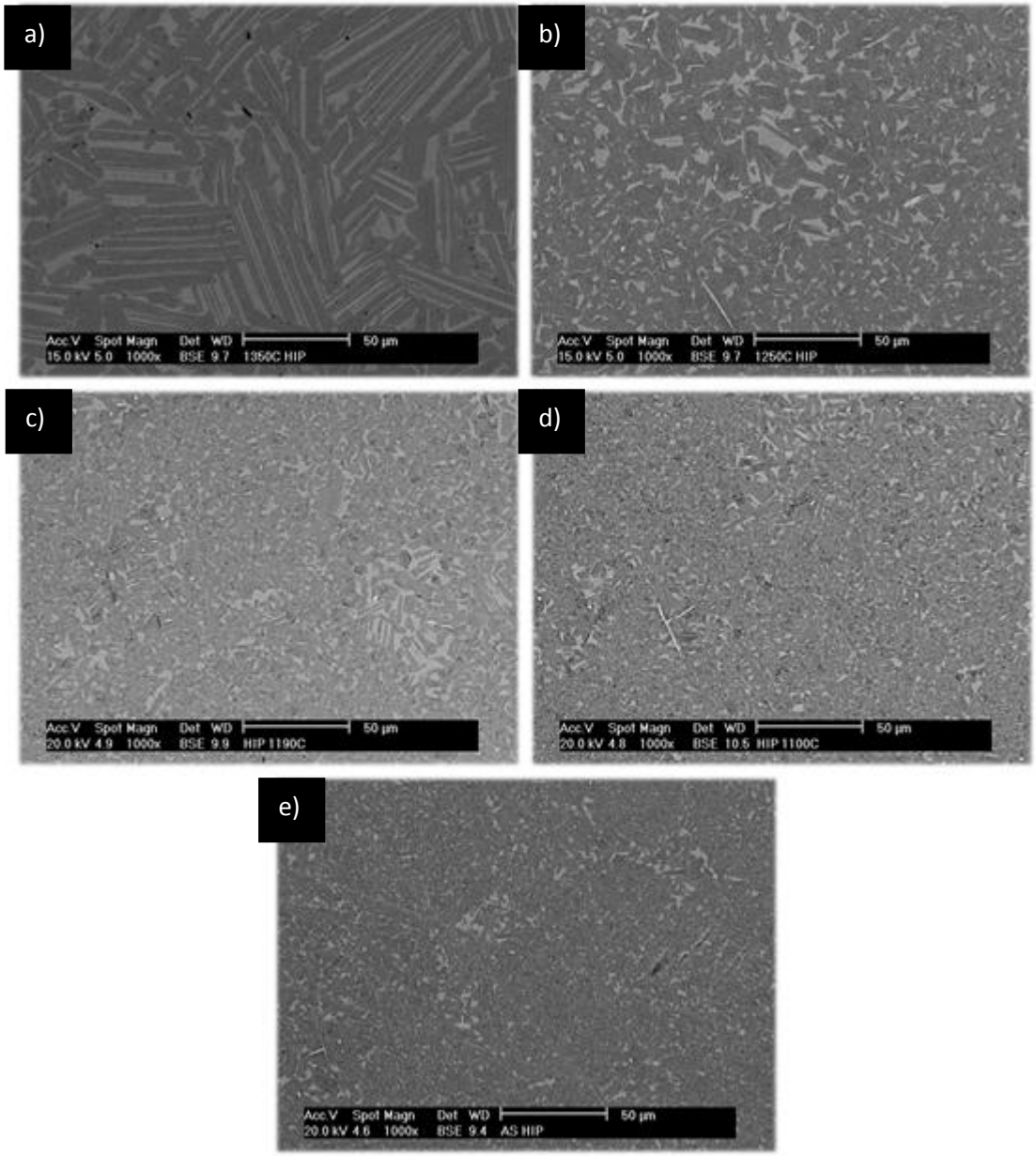

Figure 21: Images of the HIP samples taken from the SEM at 1000x, heat treated at a) 1350 °C, b) 1250 °C, c) 1190°C, d) 1100 °C and e) as HIP

Although in figures 22, 23 and 24 some lamellae are shown, the as HIP sample (figure 21-e) and the ones heat treated at 1100 °C (figure 21-d) and 1190 °C (figure 21-c) are characterized mostly by γ and α_2 grains. Therefore, these microstructures would be classified as near gamma.

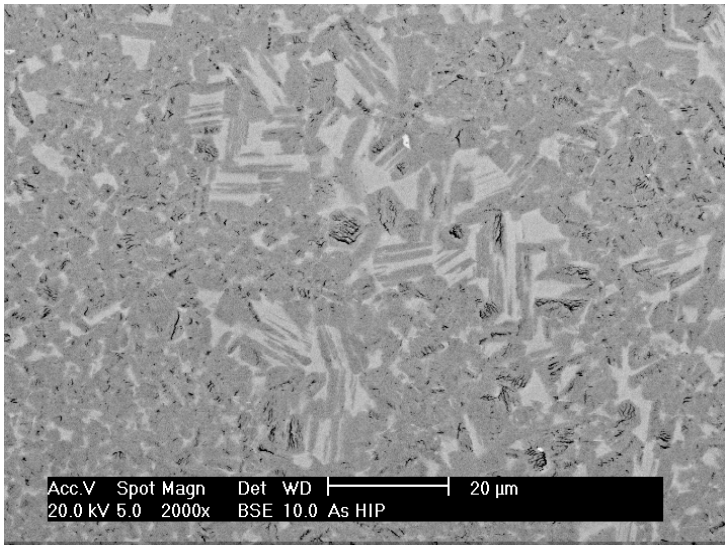

Figure 22: Image of the as HIP sample taken from the SEM at 2000x.

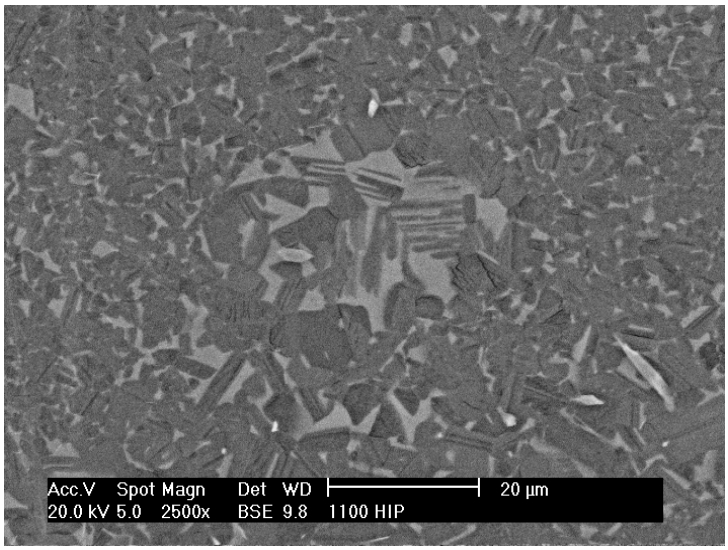

Figure 23: Image of the HIP sample taken from the SEM at 2500x, heat treated at 1100 °C

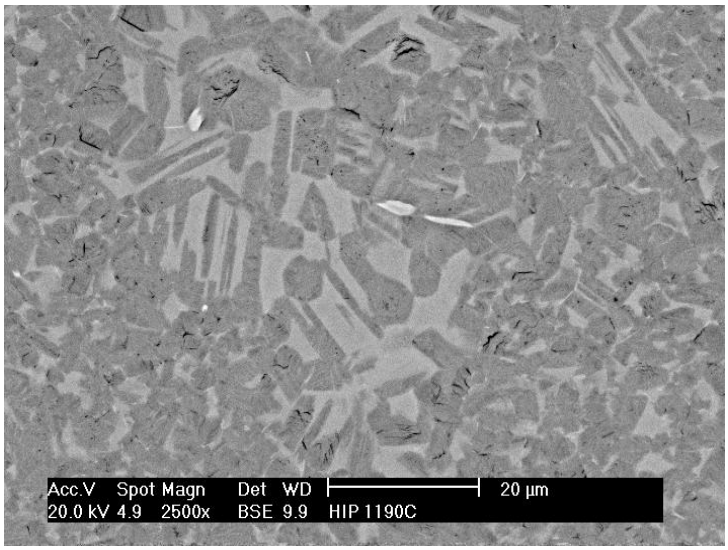

Figure 24: Image of the HIP sample taken from the SEM at 2500x, heat treated at 1190 °C

In the HIP samples as it was previously mentioned, mostly at high magnifications small cracks seem to be appearing in the γ grains also observed with SE (see figures 22, 24 and 25). At a heat treating temperature of 1250 °C (figure 21-b), it could be considered also a near γ microstructure. In figure 25, it is seen how some lamellae try to appear although not enough α was previously formed and they cannot complete the transformation.

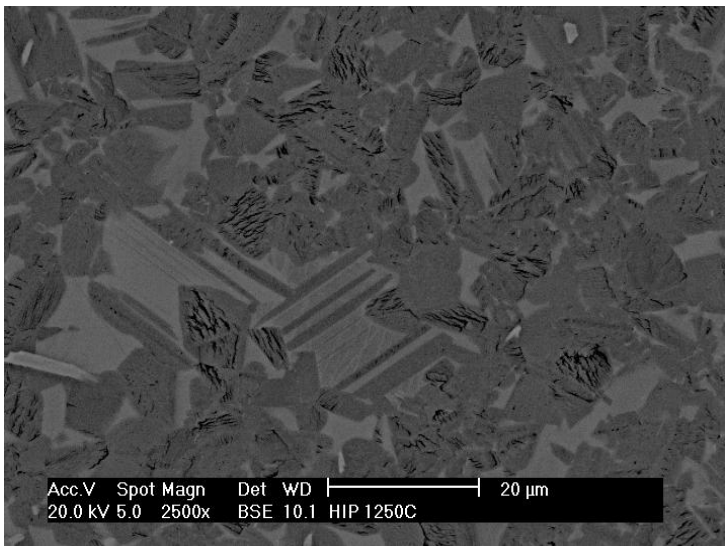

Figure 25: Image of the HIP sample taken from the SEM at 2500x, heat treated at 1250 °C

Only in those samples heat treated at 1350 °C (figure 21-a), the microstructure appears to be duplex. Some γ grains are still observed in figure 26. The results of the HIP specimens are also similar to what was reported in [16] by R. Muñoz Moreno. At 1300 °C for 2 h, the microstructure is duplex and the as HIP sample was considered near γ.

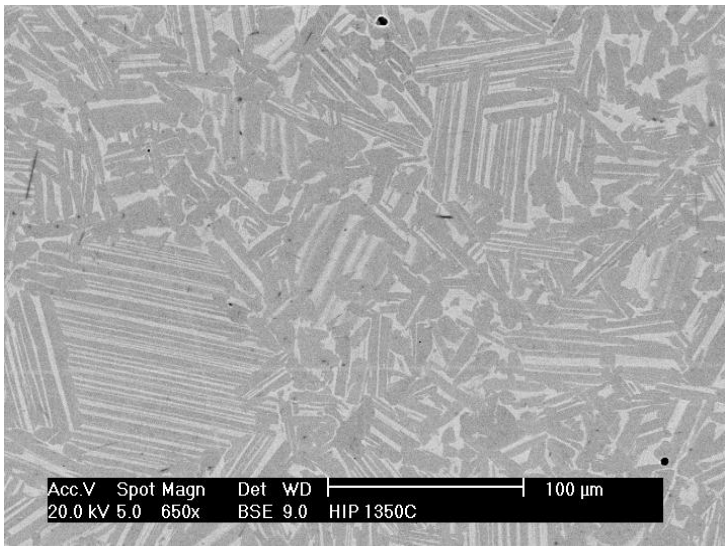

Figure 26: Image of the HIP sample taken from the SEM at 650x, heat treated at 1350 °C

CC vs. HIP SEM microstructure

From figures 17-26, the microstructures are very different between the HIP and the CC Ti4522XD alloys. As C. Yang reported in [16], with the same alloy, HIP at different temperatures in the different phase fields gives rise to very different microstructures. Therefore, the initial

treatment at which the material is processed will design the type of microstructure that will form during subsequent heat treatments. The HIP material comes from powders consolidated at 1200 °C whereas the CC samples come from superheated TiAl that is melted, poured and then, consolidated at 1185 °C. The heat treating temperature is almost the same although the origin of the material is different. When the alloy is molten and poured during the centrifugal casting it crosses all the different phase fields of the phase diagram allowing the lamellar microstructure formation. In the case of the HIP material, the powder is heated and consolidated in solid state up to 1200 °C and solid transformation occurs. Therefore, in HIP material few lamellae can only appear from (α + γ) phase field. Therefore, when the as CC or as HIP samples are heat treated, the resulting microstructures are very different at the same temperature. In the CC material, there is always lamellar microstructure present because it was previously originated in the as CC specimen. However, in the HIP material, there is only lamellar microstructure when the temperatures that can lead to it are reached (≥ T_α).

3.1.2. AFM

CC AFM microstructures

In figure 27, the images obtained by the AFM are shown for the CC sample heat treated at 1350 °C. The brighter the feature the higher it is in Z (height) axis. Apart from the lamellar colonies, areas of large grains can be distinguished. Furthermore, the high resolution allowed by this technique in the topography makes the polishing lines reveal and the rests associated to this polishing appear in figure 27-a. When it is magnified in other regions, the resulting topography is cleaner (figure 27-b). It is also shown in figure 27-d an amplitude image drawn by the recorder amplitudes developed in the oscillation of the cantilever. This image is very useful to limit the boundaries of the lamellae. Therefore, they were used for the measurement of the lamellar spacing. It was reported by Gebhard et al. [37] and Göken et al. [43] that due to the higher hardness of the α_2 phase, it is the one elevated in the topography rather than the γ-phase which appears depressed. The depressed γ-phase is also the one that presents a more uniform and planar surface in comparison to the roughness observed in the α_2 phase. The mean lamellar spacing measured for this sample in figure 27 was $\lambda_{\gamma/\alpha_2}$= 1.041 ± 0.603 µm.

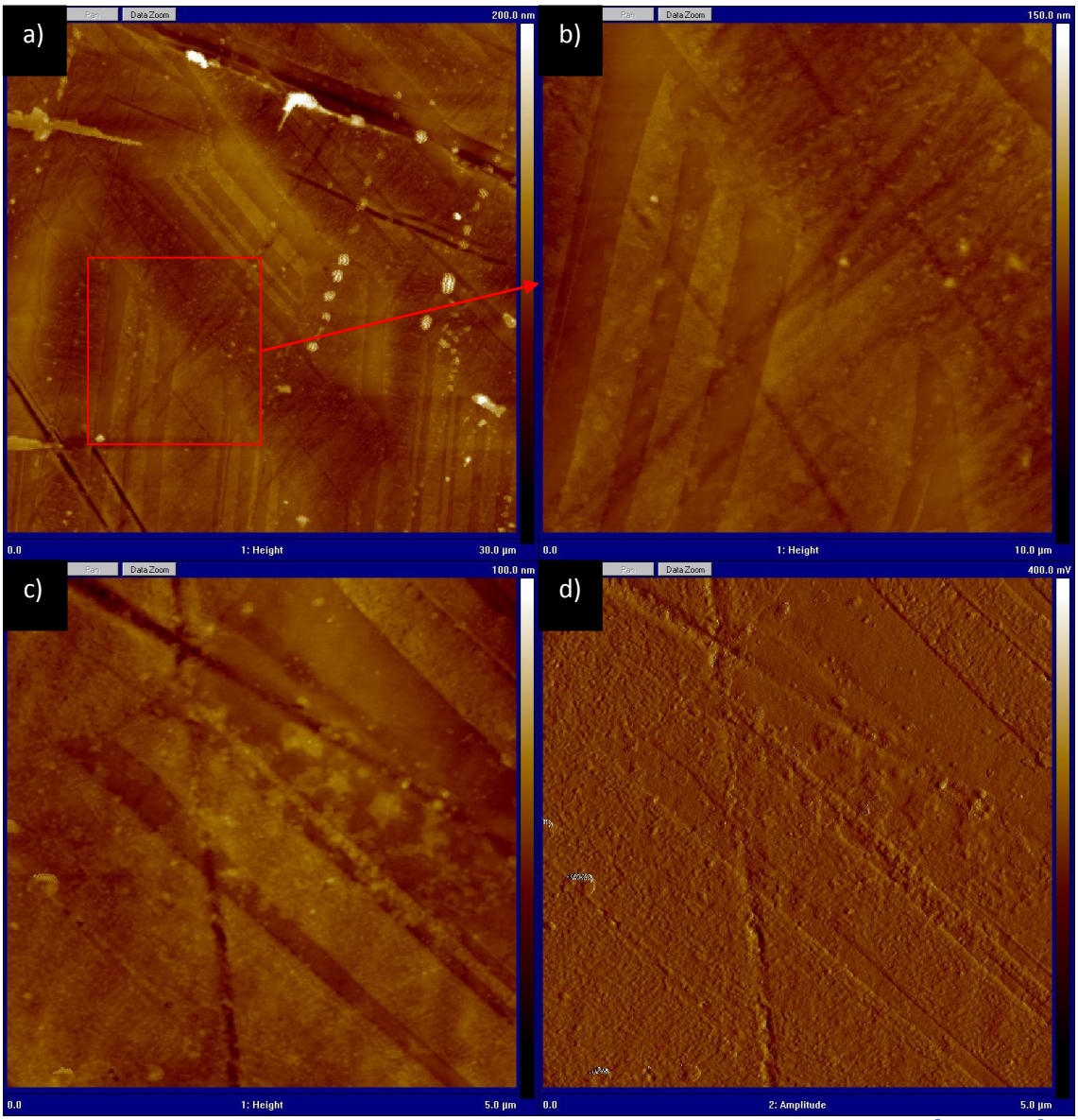

Figure 27: AFM topography images of CC sample heat treated at 1350 °C over a surface of a) 30 µm^2, b) 10 µm^2, c) 5 µm^2 and d) amplitude AFM image of 5 µm^2.

In figure 28, the intersection between two lamellae is observed. The difference of heights is of barely 5 nm.

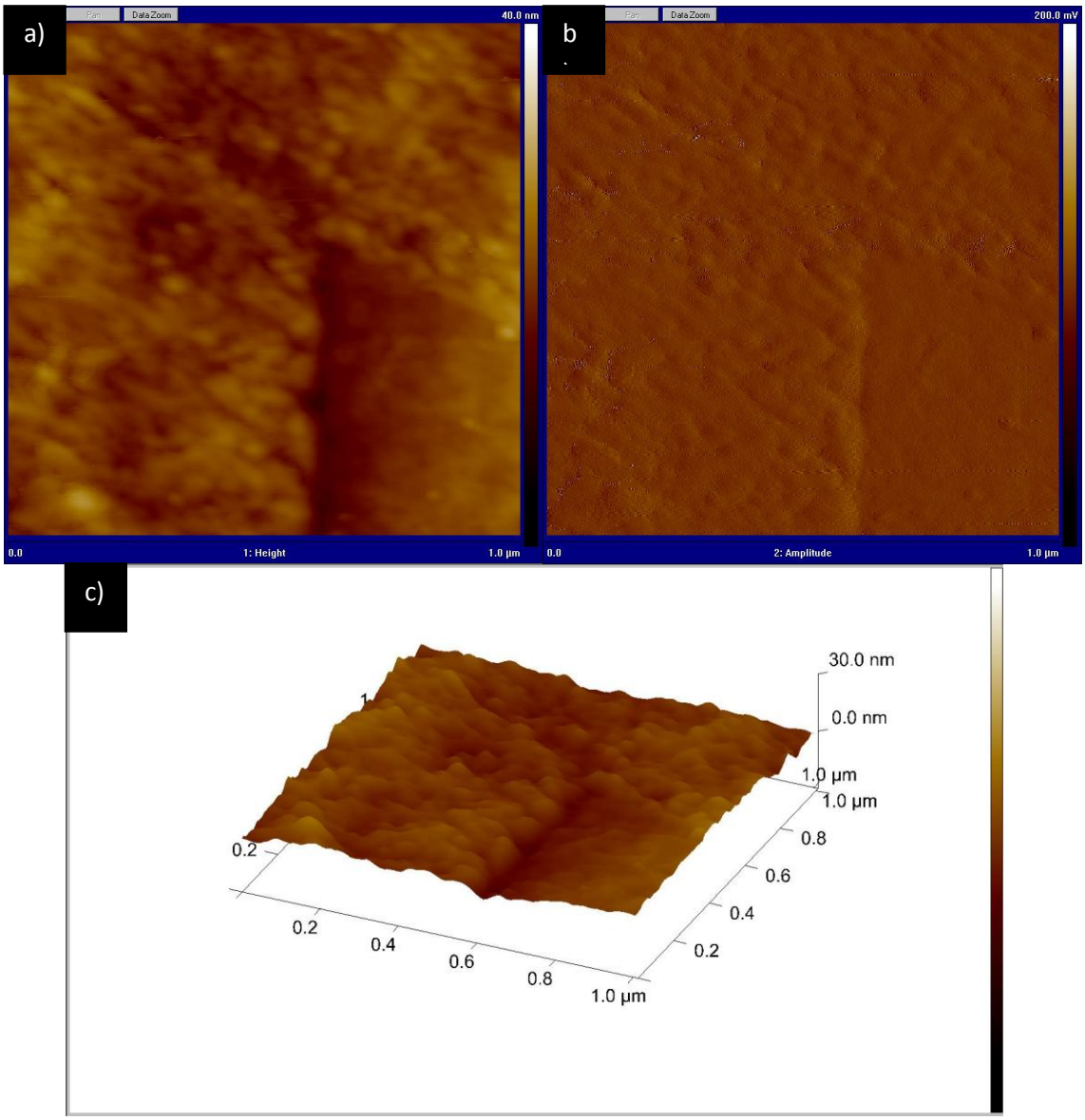

Figure 28: AFM images of the intersection between to lamellae of the CC sample heat treated at 1350 °C and of 1 µm^2. They correspond to the a) topography b) amplitude and c) topography in 3D.

HIP AFM microstructure

Regarding the HIP sample heat treated at 1350 °C, the results in terms of the roughness are opposite (figure 29) when compared to CC-1350 °C. The more planar surface corresponds to the α_2-phase. However, the depressed γ-phase presents higher roughness. Small cracks or impurities are observed in this last phase coinciding with the SEM HIP results and confirming that the depressed phase corresponds to γ. Their orientation was measured using imageJ. The angle between the crack and the boundary of the lamella was measured to be approximately 21°. The mean lamellar spacing was harder to determine due to the blur boundaries that appear in the image. The result was $\lambda_{\gamma/\alpha_2}$= 1.832 ± 1.139 µm.

The measured lamellar spacing was representative only of the scanned surface. Therefore, in both CC and HIP cases, the results cannot be extended to the entire sample. Moreover, as the

information that is provided by the AFM is the topography, the phase identification could only be determined by previous research. Therefore, in this technique only the surface is analysed and the orientation of the different microconstituents is lost in one plane. In order to measure lamellar spacing, transmission electron microscope (TEM) would be more suitable. Nevertheless, detail characteristics of the phases such as roughness could not have been observed without AFM.

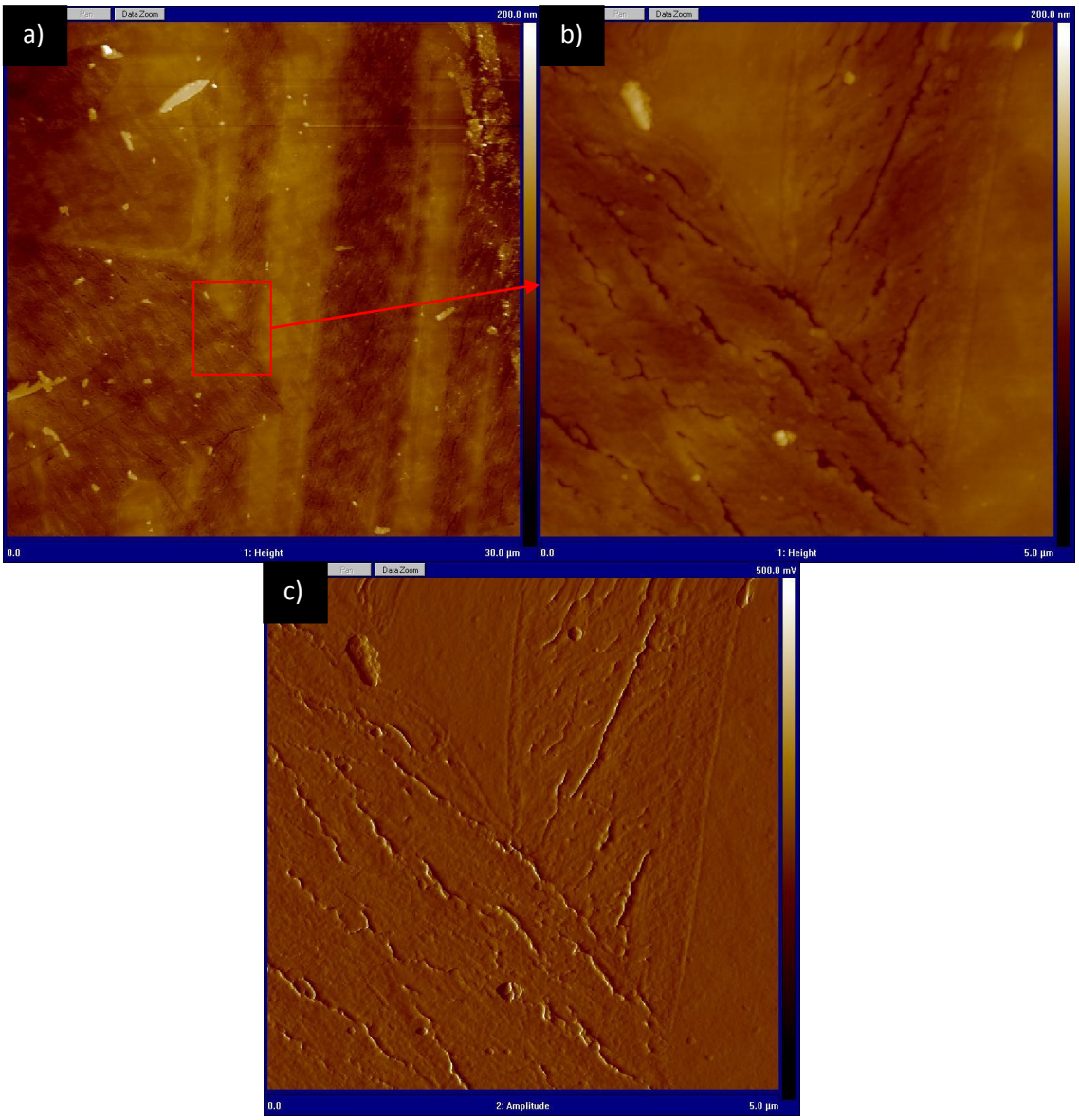

Figure 29: AFM topography images of HIP sample heat treated at 1350°C over a surface of a) 30 µm^2 and b) 5 µm^2 and c) amplitude image of the 5 µm^2.

3.1.3. Image analysis

Grain size characterization

In figures 30, 31 and 32, the grain sizes (GS) and colony sizes (CS) are analysed for all temperatures. In general, it is observed a decrease in the GS with a decrease of the heat

treating temperature. In addition to this, from the histograms it is also observed that the size of the grains of the CC samples is larger than the HIP ones. Samples heat treated at $T < T_e$ or near T_e present similar GS, although these values are significantly different when they are heat treated near T_{α}.

In the case of the lamellar colonies (figure 30), the HIP specimens have a smaller colony size than CC samples, disappearing completely when the eutectoid temperature is not reached. The increasing trend is explained with the heat treated temperature. At higher temperatures, there is more α phase that can be transformed to lamellae. Concerning the CC samples, the size is almost similar for temperatures closed to the T_{α}. The original specimen was processed at 1185 °C. The colonies in the as CC sampled are smaller than the ones heat treated at 1190 °C. This could be due to the coarsening of the existing colonies during the heat treatment at 1190 °C.

In comparison to the work presented by R. Muñoz Moreno [17], the colony sizes of her research and this present work (figure 30) are similar because the present results enter in the range stated in her thesis. In the as CC samples, the colony size was reported to be 194 ± 121 µm (ranging from 52 to 636 µm) and in the CC samples heat treated at 1300 °C, CS = 183 ± 83 µm (ranging from 80 to 463 µm) [17]. The results t in the HIP samples heat treated at 1300°C are again similar. The colonies were of approximately 98 ± 34 µm (ranging from 45 to 205 µm). Therefore, considering the high standard deviations of the reviewed results and the ones obtained in this project, CS's are more closely related.

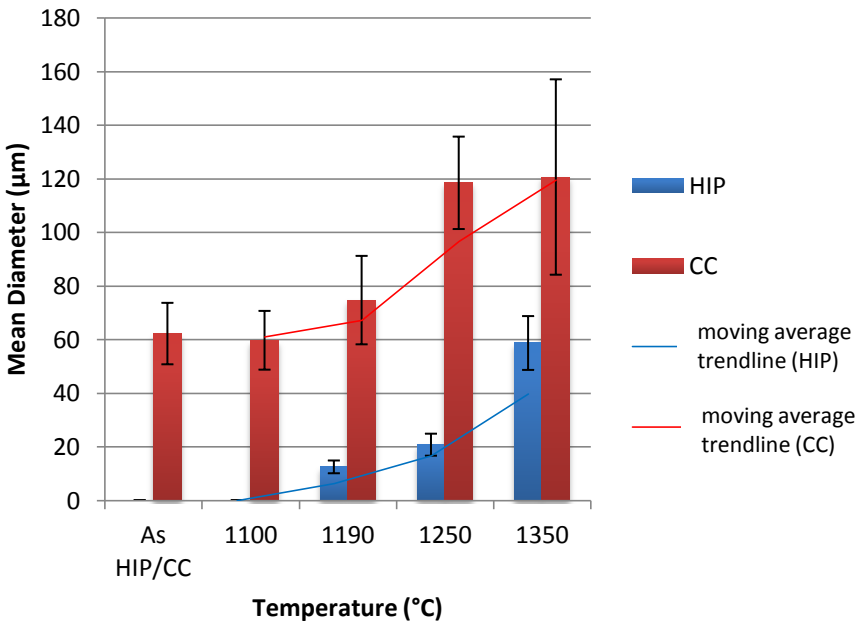

Figure 30: Lamellar colony size

In figure 31, the increasing tendency is repeated albeit at lower temperature the behaviour is different for the case of CC. In the case of the as CC samples and the ones heat treated at 1100 °C and 1190 °C, the GS remains approximately unchanged. For the case of the HIP samples the exception to the trend is only found in the material heat treated at 1100 °C which presents

smaller grain size than as HIP and the one heat treated at 1190 °C. From temperatures above 1190 °C, the GS increases considerably. Therefore, grain coarsening is produced at temperatures above the eutectoid point. In addition to this, at 1350 °C the size of the γ grains of the HIP is larger than the ones of the CC material. The GS of γ in the case of the as HIP material is comparable to what was found by R. Muñoz Moreno in [17], where it was stated to be 4.4 ± 2.6 μm (ranging from 0.6 to 11.4 μm). With respect to the sample heat treated at 1300 °C during 2h, the results do not seem to coincide reporting a GS of 4 ± 1 μm. According to figure 31, at that temperature the GS would be forecasted to be around 15 ± 5 μm.

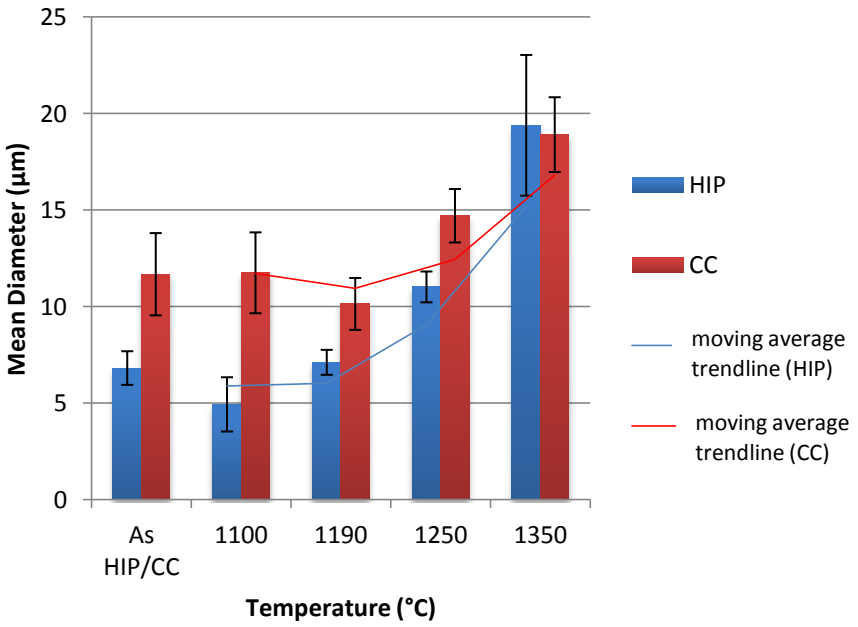

Figure 31: Size of γ grains

Finally, in figure 32 the size of α_2 grains is represented, very similar to the previous case although smaller, in general, than the γ grains. Therefore, as the temperature is increased, the α_2 grains are coarser.

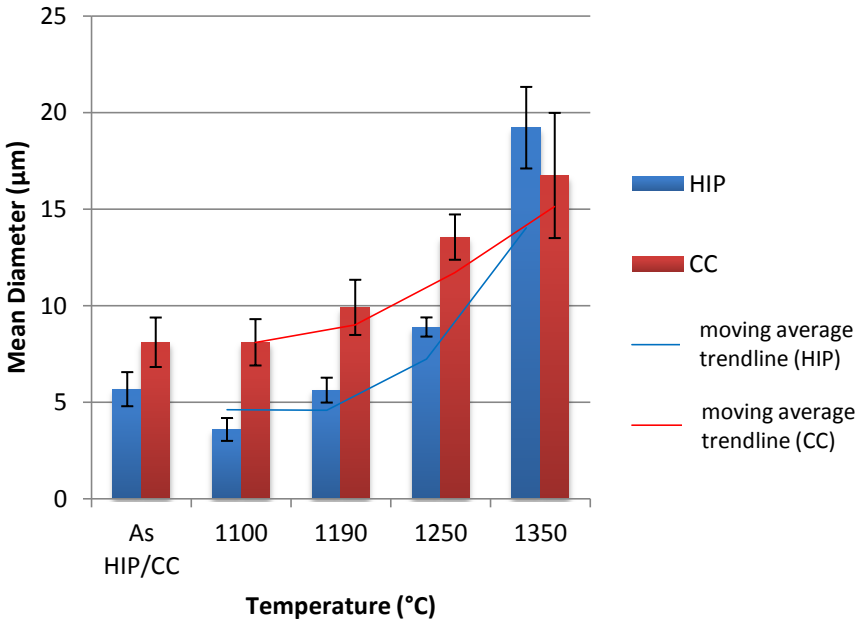

Figure 32: Size of α_2 grains

Phase distribution characterization

The volume fractions of the different phases of all materials are shown in figures 33 and 34. In both cases, CC and HIP, an important change is observed when the eutectoid temperature (1150 °C) is reached. The γ phase decreases abruptly to start increasing until T_α. Therefore, γ phase appear more abundant in the samples that were heated just below T_e, near T_α and in the as CC or as HIP materials. Moreover, the materials heated above T_e show an increase in α_2 phase. An exception to this last statement in found in the case of the as CC material where it has the highest α_2 volume fraction. In both cases, the temperature at which the fraction of γ and α_2 phases are more balanced is 1190 °C (above T_e and closed to processing temperature). In the case of the CC specimens, it is also very similar in the as CC samples (processed at 1185 °C).

As it was commented in the introduction, Appel et al [23] claimed that the HIP processing causes the γ volume fraction to be more abundant and the α_2 phase volume fraction to be smaller. If CC and HIP results are compared, it is observed that there is more γ volume fraction and, hence, less α_2 phase volume in the case of the HIP samples.

With respect to the other microstructural feature that would cover the borides, in the CC samples there is more or less the same amount except for the as CC where it is more numerous and coincides with the original composition of the processed material, 0.8 vol.%TiB_2. In the case of the HIP samples, the temperatures richer in these compounds are found to be 1250 °C and 1190 °C.

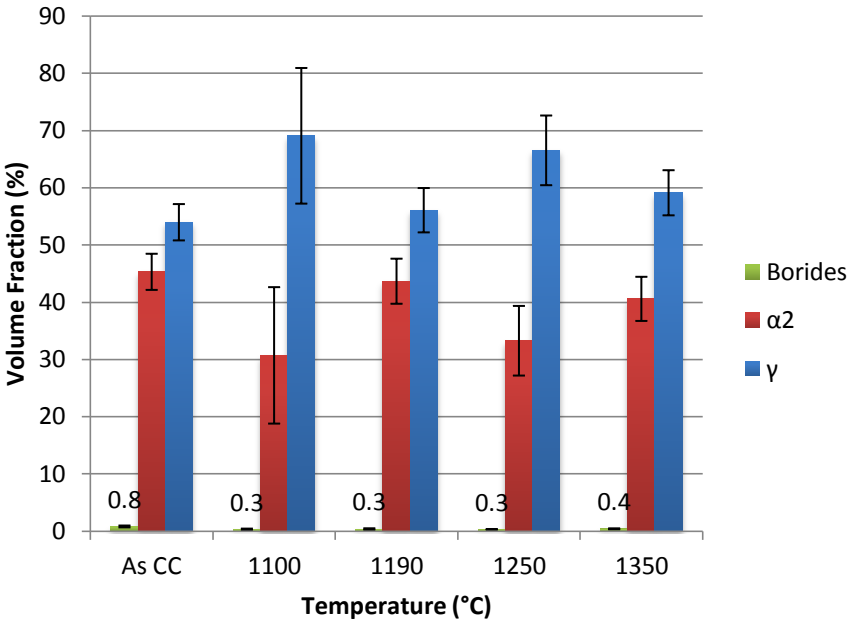

Figure 33: Percentage of phases in the CC sample

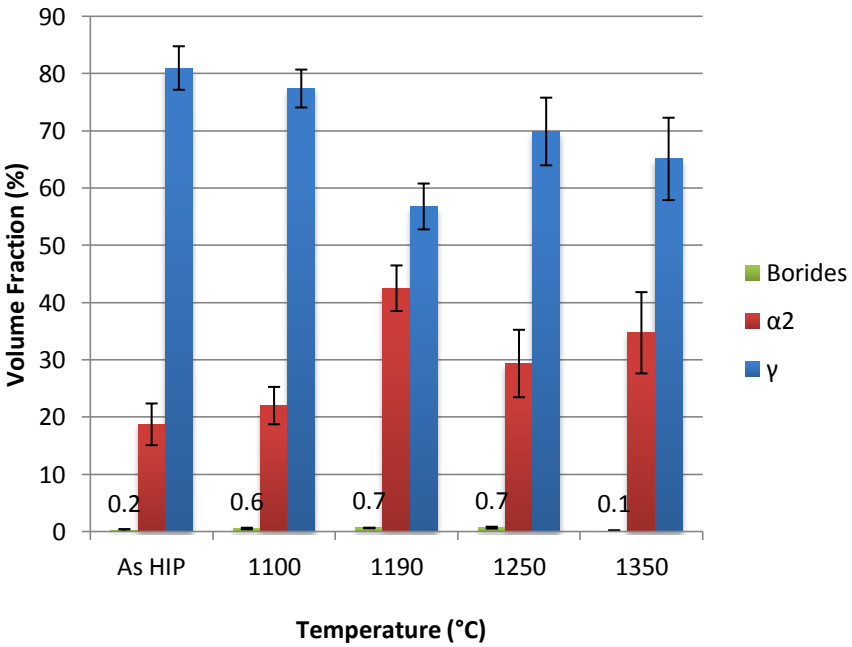

Figure 34: Percentage of phases in the HIP sample

3.2.Hardness characterization

Hardness depends significantly on the microstructure parameter as it will be explained hereafter. Figure 35 shows opposite trends around eutectoid temperature for each type of material's processing. In HIP samples, with a near gamma microstructure, the majority of the sample is formed by grains and because they are smaller and finer than the colonies, the hardness is higher (grain refinement). On the other hand, in the CC samples the lamellar

colonies appear in all the specimens with a large CS together with the γ and α_2 grains. At samples heat treated at 1250 °C, the hardness is higher for the CC samples than the HIP samples. At 1350 °C, the behaviour is again reversed. Their microstructures need to be taken into account, fully lamellar microstructures for the case of the CC and duplex microstructure for the HIP. CC hardness increase with T, when $T < T_e$ because of an increasing of the lamellae fraction. However, CC hardness decreases with T when $T > T_e$, because of a coarsening of the lamellae.

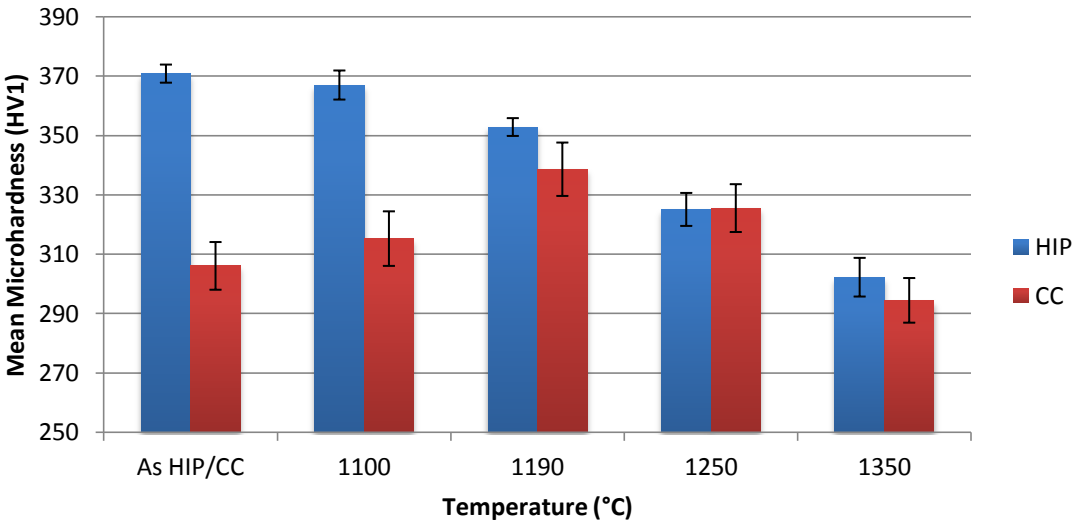

Figure 35: Microhardness Vickers test

Hardness seems to decrease as the temperature is increased. This is opposite to the results found by D.Y. Seo et al. in [8] that tested cast XD45 alloy samples with Rockwell Test and characterized it as macrohardness. This is because they refined microstructure and in the present research work coarsening of the grains is produced. Although they went only to temperatures around T_α (1400 to 1300 °C), hardness was concluded to decrease gradually as heat treatment temperature decreases because of coarse lamellar spacing and formation of equiaxed grains at lamellar grain boundaries and inside of lamellar grains [8]. In this project, the lamellar spacing is not analysed throughout the temperatures. However, the equiaxed grains are observed to appear at the grain boundaries preventing from dislocations movement and increasing the hardness.

Nevertheless, these results could be stated to be more close to reality in the case of the HIP material than the CC samples. The reason is that another parameter affecting the numbers is the relative size of the indenter in comparison to the microstructural features. More grains are affected in a single measurement in the HIP case. However, for the CC samples, the indenter easily lies on a lamellar surface or a region where more equiaxed grains are presented. In other words, in the CC samples, the indenter is actually measuring the hardness of a type of microconstituent. In addition to this, the values of the standard deviation of the hardness for the CC samples are observed to be higher than the ones coming from the HIP samples.

In order to discriminate between the hardness of a lamellar colony or other type of microconstituent, the hardness measurements at different microstructural features are carried out (figure 36).

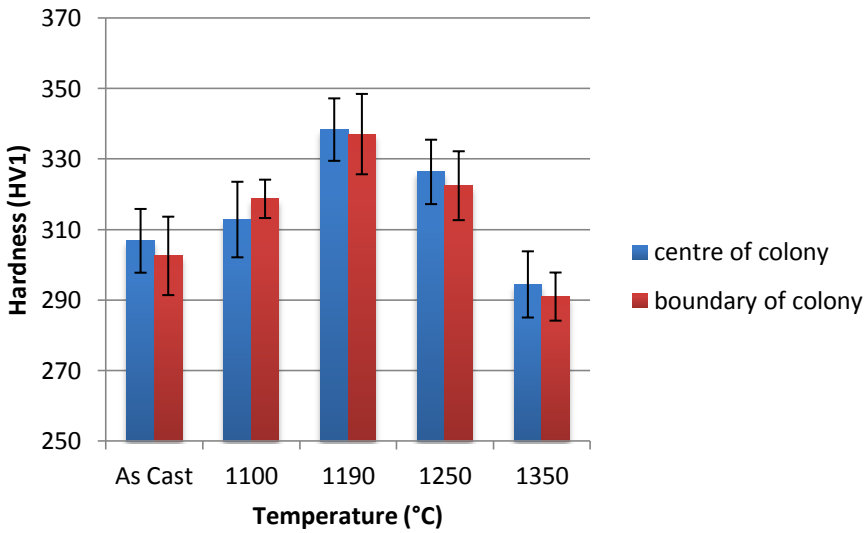

Figure 36: Microhardness Vickers test according to place of indentation of CC samples

The maximum hardness is found at 1190 °C (nearly lamellar microstructure) where equilibrium is found between the grain and colony size and the volume fraction of lamellar colonies. Moreover, it coincides with the phase distribution characterization where more α_2 was found, being this one the hardest phase [37, 43]. In general, the hardness in the centre of the colony is higher than the boundaries, confirming that the strongest microconstituent in terms of hardness response is the lamellae.

In the research works [37], [41] or [42], the Hall-Petch relation is demonstrated in equiaxed microstructure in γ-TiAl alloys. The results of microhardness together with graphs 30, 31 and 32 (GS) show that a finer grain leads to higher hardness, coinciding with Hall-Petch relation. Moreover, in [37], high strength is stated to lie in refining the lamellar size rather than the grain size when the samples being evaluated are fully lamellar TiAl-based alloys. Although the lamellae thicknesses were not measured, in the SEM images they can be observed to be finer for the case of the CC material heat treated at 1190 °C.

Nevertheless, in [42] it is stated that Hall-Petch relation seems not to be appropriated for two-phase titanium aluminide alloys because is very difficult to analyse separately and to isolate the structural parameters that play a role in the strength such as the size of equiaxed α_2 and γ grains, the colony size, lamellar spacing, domain size and the spacing of α_2 lamella. They are said to be presented with the Hall-Petch probably for simplicity.

Finally, the depth of the measurement should not be forgotten. In the optical microscope with which the Vickers Test is done, the internal microstructure cannot be seen, only the outer surface. Therefore, although to the eye what lies under the indenter seem to be a lamella, it might have also had, in a deeper level, a different microconstituent that is affecting the hardness measurement.

4. Conclusions

As a general conclusion to this work, it can be stated that the studied intermetallic composition is a good candidate to be modified through heat treatments, as have been demonstrated throughout the thesis. Different treatments can produce different well controlled microstructures which, subsequently, would be expected to influence in the final properties. With the results and their discussions the following conclusions can be drawn with respect to:

- **SEM results**

  The microstructure of Ti4522XD alloys depends greatly in the temperatures at which it is heat treated. The most important changes are not observed in relation to T_e or T_α but at the temperatures at which the raw materials were processed. Therefore, the processing of the raw material is determinant on the final microstructure.

- **AFM results**

  The difference in height of the α_2 and γ phases in the microstructure is minimum. Therefore, they are identified more easily by image contrast due to their compositions (SEM).

- **Image analysis results**

  Both the colony size and the grain size increases with increasing temperature.

  The volume fractions of the HIP and CC samples heat treated at 1190 °C are evenly distributed between both phases. The volume fraction of γ phase is more abundant than the α_2 phase for both types of processing although there is more volume fraction of γ phase in the HIP samples than in the CC samples.

- **Hardness results**

  In HIP samples, when the temperature of the heat treatment is lower, the hardness is higher due to the grain refinement. Therefore, the Hall-Petch relation is fulfilled.

  In CC samples the hardest microstructural features are the lamellar colonies. At high temperatures the lamellae coarsen and the sample loses hardness. Therefore, in the CC samples the hardness is higher when it is heated below α transus temperature due to the presence of fine lamellae and of fine equiaxed grains that prevent dislocation motion. Moreover, the large volume fraction of α_2 could also explain the increase in hardness.

5. Future Work

The following ideas are foreseen as possible works to be developed in order to do further research in Ti4522XD alloys:

- To perform TEM for further analysis of the structure of the heat treated materials. It can be alternatively done by EBSD.
- To develop nanohardness maps among the microstructures.
- To process micropillars in order to obtain the mechanical behaviour with compression tests (from room temperature up to high temperatures) and associate it with specific microstructural features.

6. References

[1] KOTHARI, K., RADHAKRISHNAN, R. and M. WERELEY, N., *"Advanced in gamma titanium aluminides and their manufacturing techniques",* Progress in Aerospace Sciences 55, Elsevier 2012, University of Maryland, USA, pp. 1-16.

[2] MORRIS, D.G. and MUÑOZ-MORRIS, M.A., "*Intermetallics: past, present and future"*, Revista de Metalurgia, Madrid 2005, vol. Extr., pp 498-501.

[3] DIMIDUK, D.M., *"Gamma titanium aluminide alloys – an assessment within the competition of aerospace structural materials",* Materials Science and Engineering A263, Elsevier 1999, Air Force Research Laboratory, USA, pp. 281-288.

[4] CLEMENS, H. and MAYER, S., *"Design, Processing, Microstructure, Properties, and Applications of Advanced Intermetallic TiAl Alloys"*, Advanced Engineering Materials 2013, 15, No. 4.

[5] VOICE, W.E., HENDERSON, M., SHELTON, F.J.E. and WU, X., "*Gamma titanium aluminide, TNB"*, Intermetallics 13, Elsevier 2005, pp. 959-964.

[6] VOICE, W., *"The future use of gamma titanium aluminides by Rolls-Royce", Aircraft Engineering and Aerospace Technology,* vol. 71, no. 4, 1999, p.337.

[7] SEO, D.Y., BEDDOES, J. and ZHAO, L., "*Primary creep behaviour of Ti-48Al-2W as a function of stress and lamellar morphology",* Metallurgical and Materials Transactions, vol. 34A, no. 10, 2003, pp. 2177-2190.

[8] SEO, D.Y., ZHAO, L. and BEDDOES, J., "*Microstructural evolution during heat treatments in Ti-45 and 47Al-2Nb-2Mn + 0.8vol.%TiB_2 XD^{TM} alloys" ,* Materials Science and Engineering A329-331, Elsevier Science, 2002, pp. 130-140.

[9] APPEL, F., D.H. PAUL, J. and OEHRING, M., *"Gamma Titanium aluminide alloys",* Chapter 2, Wiley-VCH, Science and Technology, 2011, Germany.

[10] DENQUIN, A. and NAKA, S., *"Phase Transformation mechanisms involved in two-phase TiAl-based alloys – I. Lamellar Structure Formation",* Acta mater, vol. 44, no 1, Elsevier Science, Office National d'Etudes et de Recherches Aérospatiales, 1996, France, printed in Great Britain, pp. 343-352.

[11] DEY, S.R., HAZOTTE, A. and BOUZY, E., *"Crystallographic and phase transformation mechanisms in TiAl-based alloys – A synthesis"*, Intermetallics, Elsevier, 2009, no. 17, pp. 1052-1064.

[12] MUÑOZ-MORENO, R., RUIZ-NAVAS, E.M., and others, *"Analysis of crystallographic slip and grain boundary sliding in a Ti-45Al-2Nb-2Mn (at.%)-0.8v.%TiB_2 alloy by high temperature in situ mechanical testing",* Materials Science and Engineering: A, June 2014, vol. 606, pp. 276-289.

[13] APPEL, F., D.H. PAUL, J. and OEHRING, M., *"Gamma Titanium aluminide alloys",* Chapter 5, Wiley-VCH, Science and Technology, 2011, Germany.

[14] DENQUIN, A. and NAKA, S., *"Phase Transformation mechanisms involved in two-phase TiAl-based alloys – II. Discontinuous coarsening and massive-type transformation",* Acta mater, vol. 44, no 1, Elsevier Science, Office National d'Etudes et de Recherches Aérospatiales, 1996, France, printed in Great Britain, pp. 353-365.

[15] APPEL, F., D.H. PAUL, J. and OEHRING, M., *"Gamma Titanium aluminide alloys",* Chapter 6, Wiley-VCH, Science and Technology, 2011, Germany.

[16] YANG, C., HU D., WU, A., HUANG, A., DIXON, M. "*Microstructures and tensile properties of hot isostatic pressed Ti4522XD powders"*, Materials Science and Engineering A534, 2002, pp. 268-276.

[17] MUÑOZ MORENO R., *"In-situ analysis of the high temperature deformation and fracture mechanisms of a γ-TiAl alloy"*, PhD Thesis, Department of Material Science and Engineering, Carlos III University of Madrid, March 2014, Leganés.

[18] APPEL, F., D.H. PAUL, J. and OEHRING, M., *"Gamma Titanium aluminide alloys",* Chapter 13, Wiley-VCH, Science and Technology, 2011, Germany.

[19] ZAMBALDI, C.R., "Micromechanical modelling of γ-TiAl based alloys", Fakultät für Georessourcen und Materialtechnik der Rheinisch-Westfälischen Technischen Hochschule, 2010, Aachen.

[20] Y.-W., KIM, "*Alloy design of Gamma (TiAl) Alloys*", Acta Metallurgica Sinica (English letters), 1995, vol. 8, no. 4-6, pp. 319-328.

[21] APPEL, F., D.H. PAUL, J. and OEHRING, M., *"Gamma Titanium aluminide alloys",* Chapter 14, Wiley-VCH, Science and Technology, 2011, Germany.

[22] SHOUREN, W., PEIQUAN, G. and LIYING Y. "*Centrifugal precision cast TiAl turbocharger wheel using ceramic mold"*, Journal of Materials Processing Technology 204, Elsevier 2008, pp. 492-497.

[23] APPEL, F., D.H. PAUL, J. and OEHRING, M., *"Gamma Titanium aluminide alloys",* Chapter 15, Wiley-VCH, Science and Technology, 2011, Germany.

[24] HAUTMANN, D. "*Titanium aluminide – a class all by itself*", MTU Aero engines, 1/2013, pp. 24-29.

[25] VOICE, W., *"The future use of gamma titanium aluminides by Rolls-Royce", Aircraft Engineering and Aerospace Technology,* 1999, vol. 71, no. 4 , p.337.

[26] APPEL, F., D.H. PAUL, J. and OEHRING, M., *"Gamma Titanium aluminide alloys",* Chapter 19, Wiley-VCH, Science and Technology, 2011, Germany.

[27] C. CAMPBELL, F., *"Lightweight Materials: understanding the basics"*, ASM International, 2012, p. 315.

[28] ZIPPERIAN, D., *"Colloidal Silica polishing"*, quality matters newsletter, PACE Technologies, March 2003, vol. 2, issue 3.

[29] WILLIAM D. CALLISTER, JR., "*Materials Science and Engineering: an introduction",* Chapter 4.9*, 2nd edition, John Wiley & Sons, Inc., 1991, USA.*

[30] TORRES, E.A. and RAMÍREZ A.J., "*In situ scanning electron microscopy"*, Science and technology of welding and joining, institute of materials 2011, vol. 16, no 1, pp. 68-78.

[31] "*Laboratorio de Microscopía FE-SEM*", Instituto de Ciencia de Materiales de Madrid, CSIC, accessed on 15/04/2014, <http://www.icmm.csic.es/divulgacion/posters/TEC-Microscopia%20Electronica%20de%20Barrido.pdf>

[32] SWAPP, S., "*Scanning electron microscopy*", Geochemical Instrumentation and Analysis, University of Wyoming, accessed on 15/04/2014, <http://serc.carleton.edu/research_education/geochemsheets/techniques/SEM.html>

[33] "*Microscopía electrónica*", UNED, accessed on 15/04/2014, <http://www.uned.es/cristamine/mineral/metodos/sem.htm>

[34] THORTON, J. et al*., "Scanning Probe Microscopy training notebook",* version 3.0, digital instruments, 2000.

[35] HAWKES, W.P. and SPENCE, J.C.H., *"Science of Microscopy",* Springer, vol. 2, chapters 14 and 16.

[36] GÓNZALEZ BENITO F.J., "*Microscopía de efecto túnel y AFM*", caracterización de materiales y defectos: otras técnicas de microscopía, Carlos III University of Madrid, Leganés.

[37] GEBHARD, S., PYCZAK, F. and GÖKEN, M., *"Microstructural and micromechanical characterization of TiAl alloys using atomic force microscopy and nanoindentation"*, Material Science and Engineering, Elsevier, 2009, pp. 235-241.

[38] *"Image processing solutions for material science applications",* Olympus, accessed on 24/06/2014, <www.lri.se/pdf/olympus/analySISFamily.pdf>

[39] "*ImageJ*", documentation, accessed on 01/06/2014, <http://imagej.nih.gov/ij/docs/index.html >

[40] WILLIAM D. CALLISTER, JR., "*Materials Science and Engineering: an introduction",* Chapter 6.10, 2nd edition, John Wiley & Sons, Inc., 1991, USA.

[41] TAKEUCHI, S., "*The mechanism of the inverse Hall-Petch relation of nanocrystals*", Elsevier, Scripta Materialia, 2001, Japan, vol. 44, 1483-1487.

[42] APPEL, F., D.H. PAUL, J. and OEHRING, M., *"Gamma Titanium aluminide alloys",* Chapter 7, Wiley-VCH, Science and Technology, 2011, Germany.

[43] GÖKEN, M., KEMPF, M. and NIX, W.D., "*Hardness and modulus of the lamellar microstructure in PST-TiAl studied by nanoindentations and AFM*", Elsevier, Acta Materialia 2001, no. 49, pp. 903-911.